Marine Geology 465 (2023) 107147

Contents lists available at ScienceDirect

Marine Geology

journal homepage: www.elsevier.com/locate/margo

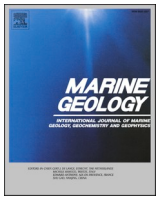

Invited research article

Contourite stratigraphic models linked to the light intermediate versus dense deep Mediterranean water flow regime variations (Alboran Sea, SW Mediterranean)

Belén Alonso [a], Gemma Ercilla [a,*], Carmen Juan [b], Nieves López-González [c], Isabel Cacho [d], Guillermo Francés [e], Desirée Palomino [c], Patricia Bárcenas [c], Mariano Yenes [f], José Nespereira [f], Blanca Ausín [f], Pilar Mata [g], David Casas [a]

[a] Institut de Ciències del Mar ICM-CSIC, The Continental Margins Group-GMC, Passeig Marítim de la Barceloneta 37-49, 08003 Barcelona, Spain.
[b] Instituto Español de Oceanografía, CSIC, Centro Oceanográfico de Cádiz, Puerto Pesquero, Muelle de Levante s/n, 11006 Cádiz, Spain
[c] Instituto Español de Oceanografía-CSIC, Centro Oceanográfico de Málaga, Puerto Pesquero s/n, 29640 Fuengirola, Málaga, Spain
[d] GRC Geociències Marines, Facultat de Ciències de la Terra, Universitat de Barcelona, Martí Franqués s/n, 08028 Barcelona, Spain
[e] Facultad de Ciencias del Mar, Universidad de Vigo, Campus Universitario Lagoas, 36200 Vigo, Spain
[f] Departamento de Geología, Universidad de Salamanca, Plaza de los Caídos s/n, 37008 Salamanca, Spain
[g] Instituto Geológico y Minero de España-CSIC, Río Rosas 23, 28003 Madrid, Spain

ARTICLE INFO

Editor: Michele Rebesco

Keywords:
Contourites
Sedimentary facies
Sequences
Stratigraphy
Bottom currents
Alboran Sea

ABSTRACT

Several water masses are involved in the circulation of oceans, their bottom layers impacting on sedimentation through contourites. The majority of palaeoceanographic studies on regional contourites are performed for one water mass despite that their joint study would offer relevant clues to understand past ocean and climate interaction. This works presents for the first time a an analysis about the impact of the Light Intermediate Mediterranean (LMW) and Dense Deep Mediterranean (DMW) bottom currents on the sedimentation in the Alboran Sea (SW Mediterranean) and its paleoceanographic significance in response to climatic oscillations from the last glacial period to the Holocene. To do this, an integration of chronostratigraphical, sedimentological, and compositional data is carried out from contourites formed by those water masses. That integration enable us to define three distinct contourite stratigraphic models. (I) The contourite terrace model, characterized by coarse-grained contourites, which is an archive of the interplay between the high-energy Atlantic Water-LMW interface and glacioeustasy from the Younger Dryas (YD) to the Holocene. (II) The contourite drift models, which are archives of rapid ocean-climate coupled fluctuations since 29.5 kyr. They comprise coarse-grained contourites formed by a relatively fast LMW and fine-grained contourites formed by a relatively weak DMW, except for the Heinrich Stadials HS3 to HS1 and YD when coarse-grained contourites were deposited. (III) The contourite/turbidite mixed model represents another archive of DMW and glacioeustasy interplay from the end of the late Pleistocene to Holocene.

That contourite stratigraphy allows us to infer for the first time the relative variability of the LMW versus DMW flow regimes, which records differences and similarities. The similarities indicate that the LMW and DMW fluctuations occur in parallel at millennial and centennial time scales. The differences refer to the overall higher velocity of LMW versus DMW; the magnitude changes in velocities that are lower for LMW and higher for DMW; the recognition of three short ventilation events (a, b, c) during HS1 and HS2 for only DMW; and the distinct LMW and DMW responses to the onset of glacial conditions and return to interglacial conditions during the HSs, YD and Holocene cold periods.

The proposed contourite stratigraphic models can be applied for other areas in the Mediterranean margins to identify and correlate the LMW and DMW palaeoceanographic events throughout this sea. The findings suggest that the different water masses that make up the water column must be seriously considered to fully understand palaeoceanographic and palaeoclimatic studies based on contourites. This is because their distinct impact on sedimentation may provide new insights into their different palaeoceanographic responses to rapid climatic oscillations and their triggering mechanisms.

* Corresponding author.
E-mail address: gemma@icm.csic.es (G. Ercilla).

https://doi.org/10.1016/j.margeo.2023.107147
Received 22 May 2023; Received in revised form 8 September 2023; Accepted 19 September 2023
Available online 26 September 2023

1. Introduction

Ocean bottom currents play a key role in continental margin sedimentation as transport, deposition and erosion processes at large scales, forming sedimentary systems that consist of depositional and erosive morphosedimentary features (e.g., drift, terrace, moat) (Rebesco and Carmelenghi, 2008). For small-scale facies, Stow and Faugères (2008) developed an ideal contourite sequence, which is composed of five divisions, named C1 to C5, which display coarsening and fining-upward sedimentary sequences. They may also be incomplete, with not all divisions represented. They can be interpreted in terms of an increase and then a decrease in bottom current velocity. The main factors governing contourite sequences are the interplay of oceanographic processes, which are closely related to short- and long-term climate variations, basin geometry, sediment supply, seafloor topography, and proximity to ocean gateways (Alonso et al., 2016; Ercilla et al., 2022; Faugères and Stow, 1993; Martorelli et al., 2021; Rebesco et al., 2014). Therefore, contourite sequences are relevant recorders of bottom-water activity and ocean-climate coupling.

The Alboran Sea (SW Mediterranean, Fig. 1A) is a regional sea with high palaeoenvironmental and palaeoceanographic variability (i.e., Cacho et al., 2001; Pérez-Folgado et al., 2003; Rogerson et al., 2012) due to its connection with the Atlantic Ocean through the Strait of Gibraltar. In this sea, a multiple contourite depositional system (i.e., contourites formed by different water masses) characterizes deep sedimentation (i.e., environments beyond the continental shelf edge) during the Plio-Quaternary (Ercilla et al., 2016; Juan et al., 2016, 2020). This multisystem developed under the interaction of the entering Atlantic Water (AW) and the outgoing Mediterranean Water (MW) masses, the latter involving the Light Intermediate MW (LMW) and the Dense Deep MW (DMW) (Fig. 1A; Ercilla et al., 2016). The Quaternary depositional architecture of contourites reflects the complexity of MW (palaeo)circulation interacting with tectonics and the progressive variations in the Alboran basin configuration, local seafloor topography, sea level changes and climatic variability. The recent palaeoceanography of DMW has received major attention in recent years based on geochemical, palaeontological and sedimentological analyses (e.g., Alonso et al., 2021; Ausín et al., 2015; Bazzicalupo et al., 2020; Cacho et al., 2000, 2001; Català et al., 2019; Jimenez-Espejo et al., 2007; Martrat et al., 2004; Moreno et al., 2005; Nebout et al., 2009; Nieto-Moreno et al., 2011; Rodrigo-Gámiz et al., 2018; Sierro et al., 2005). These studies have demonstrated that millennial- and centennial-scale climate cycles and related sea surface temperature variations induced rapid changes in DMW oceanographic conditions via oscillations in thermohaline circulation. In contrast, LMW palaeoceanography has received little attention in the Alboran Sea (Jimenez-Espejo et al., 2008; López-González et al., 2019; Pérez-Asensio et al., 2020). Therefore, there is a need to fill this gap to understand the LMW and DMW coupling in relation to ocean-climate variability. This is relevant because palaeoceanographic models suggest that the Mediterranean Outflow Water (MOW) plays a critical role in the N Atlantic climate (Bigg and Wadley, 2001; Rogerson et al., 2005). Its relevance is explained because the MOW involves the outflow of LMW and DMW, with LMW being the major contributor (90% of MOW) (Kinder and Parrilla, 1987; Millot, 2013).

This study mainly focuses on chronostratigraphic, sedimentological and compositional analyses of sediment cores retrieved from different contourite features (terrace and drifts) in the NW Alboran Sea combined with an ad hoc support of current meter records. The main aim is to decipher the LMW and DMW palaeoceanography during the last glacial-Holocene. To this end, the characterization of the contourite stratigraphic models that comprise the sedimentary architecture are fundamental to gaining new insights into the magnitude of the millennial- and centennial-scale fluctuations in bottom currents and their palaeoclimatic significance. The analysis of the similarities and differences in the drift facies and stratigraphic models will help to address whether climate changes had a differentiated impact on LMW and DMW bottom current dynamics.

2. Regional setting

2.1. Oceanographic and palaeoceanographic settings

The oceanographic setting of the Alboran Sea is defined by the eastwards-flowing AW that enters from the Atlantic Ocean via the Strait of Gibraltar moving at up to 100 cm/s and flowing in two anticyclonic gyres down to 150–250 mwd (metres water depth; Fig. 1A; Millot, 1999; Parrilla et al., 1986). Below, four Mediterranean Water Masses (MWs) moving towards the Strait of Gibraltar are characterized; from top to bottom they are Western Intermediate Mediterranean Water-WIW, Levantine Intermediate Water-LIW, Tyrrhenian Deep Water-TDW, and Western Mediterranean Deep Water-WMDW (Fig. 1A; Millot, 2014; Millot and Monaco, 1984). These are grouped into two main water masses, light and dense (Fig. 2A; Ercilla et al., 2016). The Light Mediterranean Water (LMW) comprises the WIW and LIW and extend down to 600 mwd, and its nearly bottom layer flows mainly along the Spanish continental slope up to 14 cm/s (Ercilla et al., 2016). The Dense Mediterranean Water (DMW) is composed of the TDW and WMDW, and it is mostly concentrated along the African margin and deep basins and advance at pulses of 22 cm/s (Fig. 1A; Ercilla et al., 2016; Fabres et al., 2002; Gascard and Richez, 1985).

During the last glacial period, the Alboran Sea underwent rapid oscillations in hydrographic conditions owing to abrupt climatic changes recorded in the Northern Hemisphere, known as Heinrich stadials (HSs), which were described as cold temperature intervals during Heinrich events (Barker et al., 2009), and Dansgaard–Oeschger (D-O) Stadials (cold) and Interstadials (warm) (Dansgaard et al., 1993; Heinrich, 1988). These findings indicate a strong link between the Mediterranean and N Atlantic climate (Cacho et al., 2001; Martrat et al., 2004; Moreno et al., 2002; Sierro et al., 2005). HS and D-O cycles in marine records of the western Mediterranean Sea have been associated with synchronous oscillations of sea surface temperatures and changes in Mediterranean deepwater convection (Cacho et al., 2000; Sierro et al., 2005; Skliris, 2014). This rapid connection between both regions has been interpreted to result from the entrance of cold surface waters into the Mediterranean Sea through the Strait of Gibraltar but also from the intensification of atmospheric circulation (Cacho et al., 2000).

2.2. Geological setting

The Alboran Sea developed in a convergent tectonic setting between the Eurasian and African plates (Carminati et al., 2012; Comas et al., 1992; Vázquez et al., 2021). It is a semienclosed sea bordered by the Iberian margin to the north and the African margin to the south (Fig. 1A). The present-day physiography of the Iberian margin is defined by four physiography domains. A continental shelf extends down to 95–115 mwd; an irregular continental slope extends down to 575–945 mwd; a local base of slope extends down to 600–945 mwd; and a deep basin is located at 900–1510 mwd (Fig. 1B and C; Ercilla et al., 2016). Sedimentation is mostly siliciclastic, which is mainly derived from river discharge capable of carrying material directly to the coast or aeolian dust pulses from the African margin (Fabres et al., 2002; Jimenez-Espejo et al., 2008; López-González et al., 2019; Moreno et al., 2002; Rodrigo-Gámiz et al., 2014). Bioclasts (foraminifers, diatoms, etc.) from oceanic primary palaeoproductivity is mainly controlled by upwelling and trade winds related to climatic cyclicity during the Upper Quaternary (Cacho et al., 2000; Moreno et al., 2004). Furthermore, glaucony grains have been documented on sediments of the outer shelf and upper continental slope (50 to 225 mwd) in NW Alboran Sea (Domínguez et al., 1998; Ercilla et al., 1994).

Plio-Quaternary seismic stratigraphy reveals the ubiquity of contourite deposits (Ercilla et al., 2016, 2019; Juan et al., 2016), revealing the important impact of bottom current action on sedimentation in the

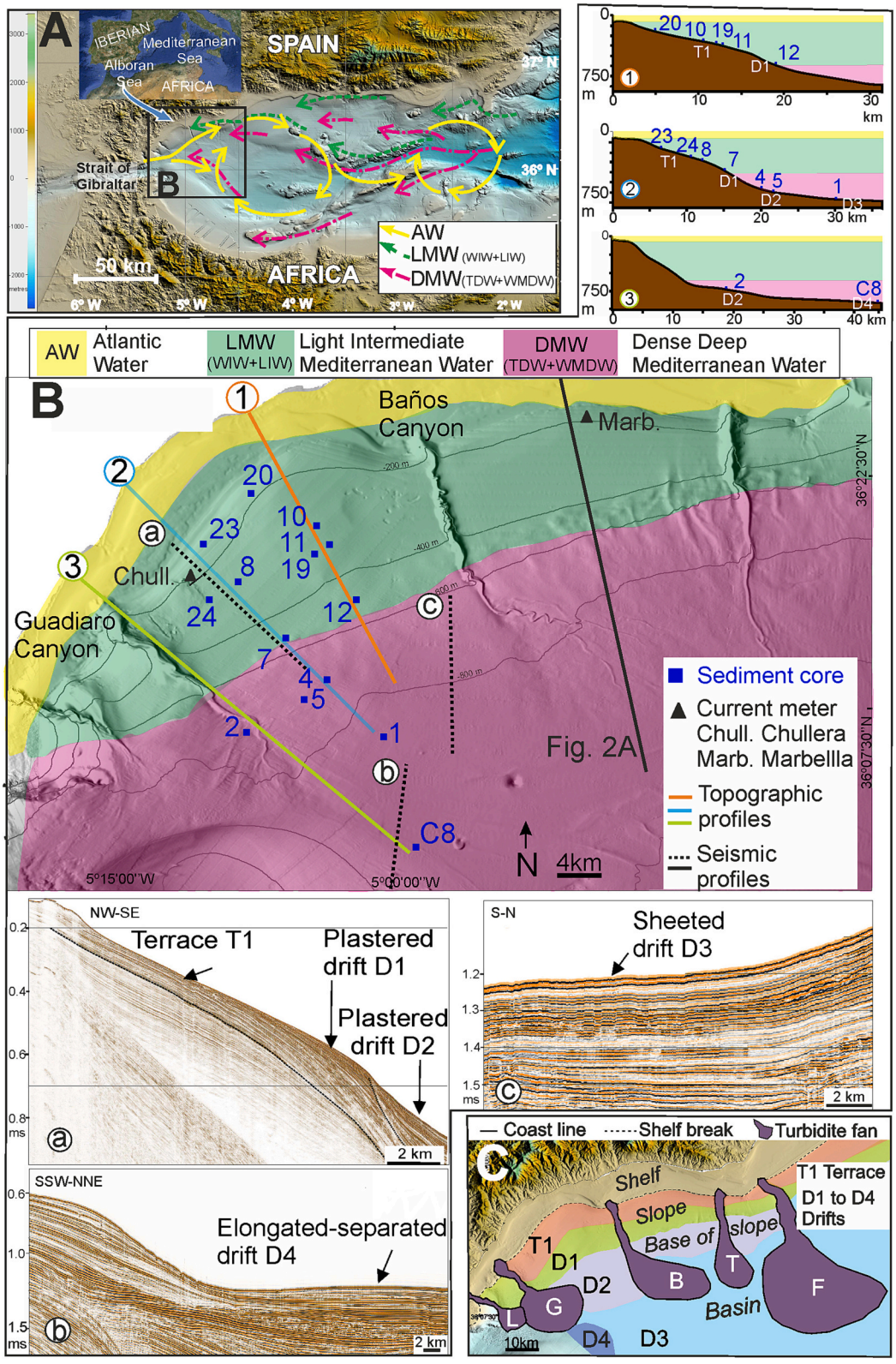

Fig. 1. Location of the study area in the NW Alboran Sea and datasets used in this work. (A) Regional hydrography of the Alboran Sea (modified from Ercilla et al., 2016) showing the present-day circulation model of the Atlantic Water (AW), the Light Intermediate Mediterranean Water (LMW) and the Dense Deep Mediterranean Water (DMW). (B) Bathymetric map with the near-bottom water mass distribution illustrating the location of the fourteen sediment cores and the two current metrers that are analysed in this study. Likewise, (B) shows three seismic profiles (a, b, and c) that display the contourite terrace and drifts that have been studied; ii) three topographic profiles (1, 2, and 3) that show the vertical positions of AW, LMW and DMW and core locations. (C) Cartography of contourite features (terrace T1 and drifts), turbidite fans and physiographic provinces based on Ercilla et al. (2016) and Yenes et al. (2021). Legend: F Fuengirola; T Torrenueva; B Baños; G Guadiaro; L La Linea.

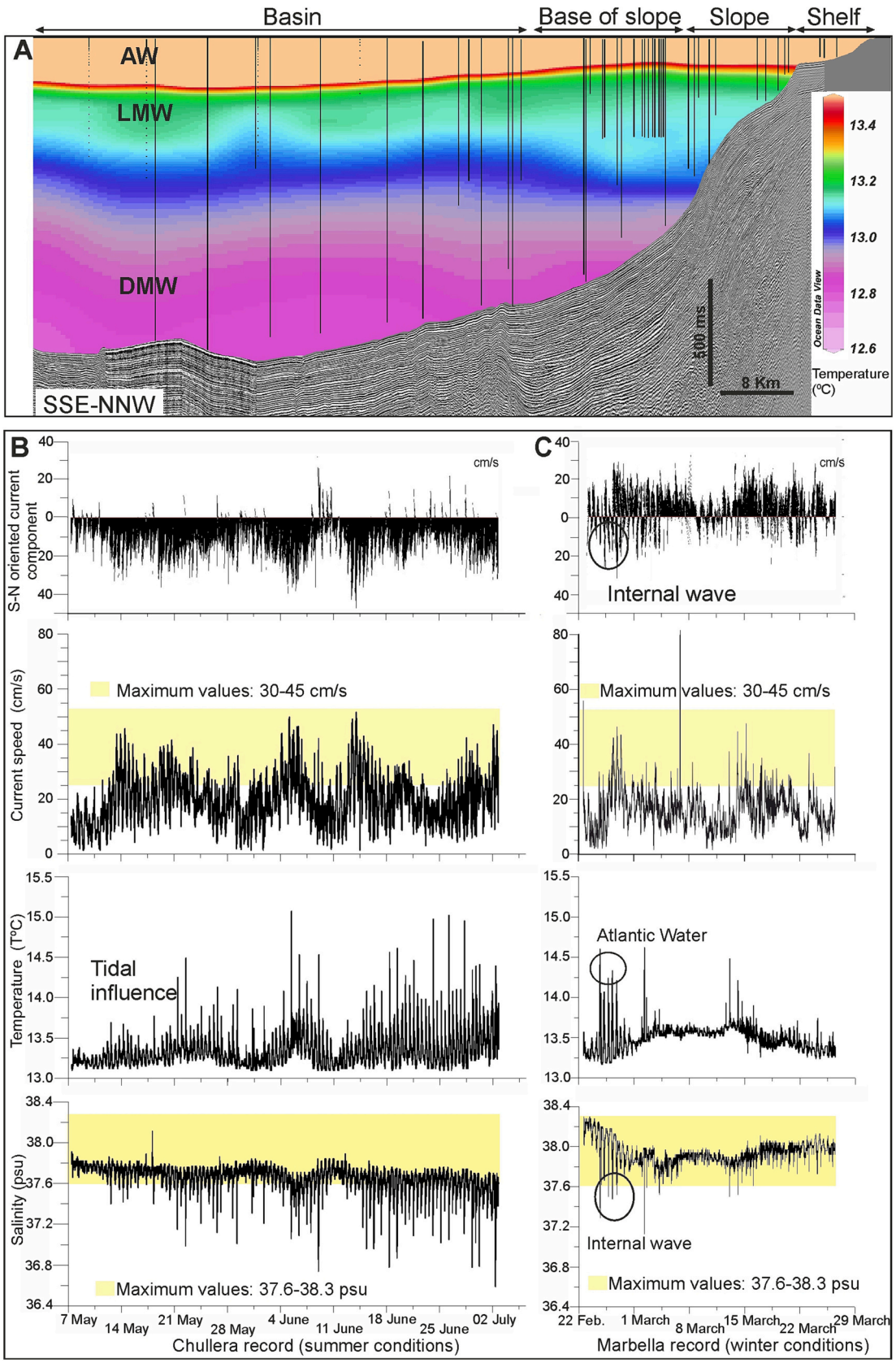

Fig. 2. Characteristics of the Atlantic Water (AW), Light Intermediate Mediterranean Water (LMW), and Dense Deep Mediterranean Water (DMW) together with current meter measures. (A) Seismic-hydrographic profile indicating the temperature of AW, LMW and DMW; the black vertical lines within the water column indicate the water depth reached by the CTDs used for the water mass characterization (modified from Ercilla et al., 2016). (B and C) Time series of the near-bottom hydrodynamics showing hydrological parameters (oriented velocity of the current, N-0°, S-180°), current speed (module of the velocity), temperature and salinity from two current meters (Chullera and Marbella in B and C respectively).

Alboran Sea. The contourites consist of depositional (plastered, sheeted, and separated drifts) and erosive (terraces, moats, and channels) deposits. In the NW sector of the Alboran Sea, contourites coexist and interact with turbidite fans (Fig. 1C; Alonso and Ercilla, 2003; Ercilla et al., 2019). The study area is located in that sector, being limited by the Guadiaro and Baños canyons to the north and by the basin of the Africa margin to the south (Fig. 1B). That region was characterized previously by geophysical works (Ercilla et al., 2016; Juan et al., 2020) where one contourite terrace named T1 and four contourite drifts named D1 to D4 (Fig. 1B and C) were recognized (Ercilla et al., 2016; Yenes et al., 2021). Terrace T1 is formed in the upper slope by the turbulence-related processes associated with the interface between AW and LMW (the highest density contrast between waters masses in the Alboran Sea) and their shifts due to Quaternary sea-level changes (Ercilla et al., 2016). The alongslope plastered drift D1formed in the lower slope by LMW bottom current action; the plastered drift D2 along the base of slope and the basinal sheeted drift D3 by the DMW bottom current action; and the basinal drift D4 corresponds to an elongated, separated drift that was also formed by the DMW (Fig. 1B and C; Ercilla et al., 2016).

3. Materials and methods

3.1. Current meter dataset

Two different current meter datasets recorded by the IEO (Spanish Institute of Oceanography) were downloaded from the SeaDataNet portal (https://www.seadatanet.org/) (Fig. 1B). These moorings measured the temperature, salinity, speed of the current and its angle along contourite terrace T1. The Chullera current meter (Lat: 36.28 N/ Lon: 5.175 W; at 200 mwd) consisted of two devices (AANDERAA RCM4) installed at 20 and 100 m above the seafloor they were actively recording data for almost two months (from 07-05-1980 to 02-07-1980). The Marbella current meter (also AANDERAA RCM4) (Lat: 36.42 N/Lon: 4.83333 W; at 200 mwd) consisted of two devices installed at 9 and 70 m above the seafloor; they were actively recording data for over one month (from 22-02-1979 to 26-03-1979). These datasets were recorded in different years and different oceanographic contexts: in February–March (Marbella record) when winter conditions prevail and from May to July (Chullera record) when the Alboran Sea switches to summer conditions (Macias et al., 2016).

3.2. Sampling dataset

Thirteen gravity cores (1, 2, 4, 5, 7, 8, 10, 11, 12, 19, 20, 23, and 24) and one piston core (C8) were studied (Fig. 1B). Gravity cores were recovered in the framework of the FAUCES and GC-90-1 projects and the piston core was recovered in the framework of the CONTOURITE project (http://gma.icm.csic.es/sites/default/files/geowebs/OLsurveys/samples.htm). Core data are detailed in Table 1. Sediment core sampling was performed at 6 to 10 cm intervals except for cores 7 and C8, which were sampled at 2–3 cm interval to establish the age model. Core C8 was previously analysed by Ausín et al. (2015) and Alonso et al. (2021), and cores 19, 20, 23 and 24 were analysed by Ercilla (1992) and Ercilla et al. (1994).

3.3. Chronostratigraphic analysis

The age-depth model for core 7 is based on four radiocarbon (^{14}C) dates from well-preserved monospecific samples of planktonic foraminifera (*Neogloboquadrina incompta or Globorotalia inflata*) measured by accelerator mass spectrometry (AMS) at the Poznan Radiocarbon Laboratory (Table 2). The age-depth model of core C8 is based on fifteen AMS-^{14}C dates from monospecific samples of *N. incompta* and *G. inflata* published elsewhere (Ausín et al., 2015; Table 2). For both age-depth models, conventional ^{14}C dates were converted into calendar years (cal. yr BP) using the online calibration package Oxcal v 4.4.4. (Ramsey, 2008, 2009) and calibrated with the Marine20 curve (Heaton et al., 2020). A regional surface reservoir updated to a Marine20 (ΔR_{20}) of 11 $\pm$ 170 ^{14}C years was applied and obtained by averaging the 3 closest data points to our locations and extracted from the online database http://calib.org/marine/ (Reimer and Reimer, 2001). Oxygen isotope (δ18O) measurements in core 7 were obtained on monospecific samples of planktonic foraminifera *Globigerina bulloides*. The measurements were carried out by isotope-ratio mass spectrometry (IRMS) at the Scientific and Technological Centres of the University of Barcelona (CCiT-UB). For the chronostratigraphy for the rest of the cores multiple data sets have

Table 1
Location of studied cores in the NW Alboran Sea.

Core name this study	Core name	Sediment core type	Water depth (m)	Core lenght (cm)	Longitude (°W)	Latitude (°N)	Name project	Physiographic location	Present water masses	Contourite feature
1	GC1	Gravity core	841	300	−4.981688	36.12852	FAUCES	Base of slope	DMW	Sheeted drift D3
2	GC2	Gravity core	731	250	−5.121826	36.14074	FAUCES	Base of slope	DMW	Overbank GF
4	GC4	Gravity core	736	300	−5.066714	36.16528	FAUCES	Base of slope	DMW	Plastered drift D2
5	GC5	Gravity core	756	300	−5.049448	36.17068	FAUCES	Base of slope	DMW	Plastered drift D2
7	GC7	Gravity core	478	290	−5.096937	36.22752	FAUCES	Lower slope	LMW	Plastered drift D1
8	GC8	Gravity core	336	50	−5.121023	36.25385	FAUCES	Upper slope	LMW	Terrace T1
10	GC10	Gravity core	319	70	−5.066899	36.31763	FAUCES	Upper slope	LMW	Terrace T1
11	GC11	Gravity core	346	130	−5.055147	36.30327	FAUCES	Upper slope	LMW	Terrace T1
12	GC12	Gravity core	563	290	−5.022041	36.24528	FAUCES	Lower slope	DMW	Plastered drift D1
19	TG19	Gravity core	331	19	−5.068000	36.2804	GC-90-1	Upper slope	Interface AW & LMW	Terrace T1
20	TG20	Gravity core	175	22	−5.133600	36.3172	GC-90-1	Upper slope	Interface AW & LMW	Terrace T1
23	TG23	Gravity core	145	9	−5.166900	36.2844	GC-90-1	Upper slope	Interface AW & LMW	Terrace T1
24	TG24	Gravity core	303	64	−5.150200	36.2350	GC-90-1	Upper slope	Interface AW & LMW	Terrace T1
C8	PC8	Piston core	914	638	−4.871660	36.02022	CONTOURIBER	Basin	DMW	Sep. Elong. drift D4

Legend: Sep Separated; Elong Elongated; GF Guadiaro Fan.

Table 2
AMS ^{14}C radiocarbon dated levels for cores 5, 7, 8, 10, 11 and C8. The AMS ^{14}C dates were converted into calendar years (cal. yr BP) using the Oxcal and MARINE20 calibration datasets.

Core number	Sample (cm)	Species	Laboratory Code	Conventional 14C age (14C yr BP) ± 1σ	Calendar age (yr cal. BP) ± 2σ (rounded)
5	280	*N. incompta*	Poz-137318a	10,770 ± 60	12,130 ± 150
7	30	*G. inflata*	Poz-137319a	3875 ± 30	3670 ± 90
7	150	*N. incompta*	Poz-137320a	8670 ± 40	9140 ± 90
7	200	*N. incompta*	Poz-137322a	11,320 ± 60	12,670 ± 80
7	290	*N. incompta*	Poz-137323a	24,690 ± 190	28,030 ± 230
8	30	*G. inflata*	Poz-137324a	4015 ± 35	3850 ± 90
10	20	*G. inflata*	Poz-137326a	2625 ± 30	2150 ± 90
11	124	*N. incompta*	Poz-149477a	10,620 ± 60	11,760 ± 130
C8	22	*G. inflata*	Poz-56516a	5870 ± 40	6110 ± 85
C8	46	*N. pachyderma*	Poz-56517a	7940 ± 40	8220 ± 80
C8	82	*N. pachyderma*	Poz-56518a	9190 ± 50	9735 ± 110
C8	122	*N. pachyderma*	9977b	9900 ± 30	10,760 ± 110
C8	156	*G. bulloides*	9552b	11,410 ± 30	12,750 ± 65
C8	174	*N. pachyderma*	10602b	12,240 ± 70	13,560 ± 105
C8	281.5	*N. pachyderma*	9979b	14,270 ± 40	16,420 ± 115
C8	323.5	*N. pachyderma*	9980b	14,920 ± 40	17,235 ± 115
C8	406	*N. pachyderma*	9981b	16,910 ± 40	19,510 ± 125
C8	452	*N. pachyderma*	9982b	18,110 ± 50	20,920 ± 115
C8	474	*N. pachyderma*	9983b	18,360 ± 50	21,300 ± 140
C8	541.5	*N. pachyderma*	9984b	20,170 ± 50	23,240 ± 125
C8	579.5	*G. bulloides*	10603b	20,480 ± 60	23,730 ± 105
C8	603.5	*G. bulloides*	10604b	21,100 ± 60	24,390 ± 105
C8	615.5	*N. pachyderma*	10605b	21,540 ± 60	24,830 ± 145

Legend: a refers to those ^{14}C AMS age measures at Poznan Radiocarbon Laboratory (Poz), and b refers to those measures at the Center for Applied Studied of University of Georgia. Legend: *N. Neogloboquadrina; G. Globorotalia.*

been integrated and correlated. This integration includes four additional radiocarbon dates (14C) (Table 2), facies, carbonate content (%), Ca-XFR record, and age model.

3.4. Sedimentological analysis

Grain-size analysis and distribution were performed using a Coulter LS 100 laser particle size analyser on both the bulk fraction (223 samples) and noncarbonate fraction (465 samples). Grain-size statistical parameters were calculated using GRADISTAT software (Blott and Pye, 2001) and based on the geometric graphical method (Folk and Ward, 1957). The D50 (μm), the sand content, and the UP10 percentage of the noncarbonated fraction (i.e., particles coarser than 10 μm) are used as proxies of palaeobottom current intensity (e.g., Frigola et al., 2007; Martorelli et al., 2021; McCave and Hall, 2006).

3.5. Compositional analysis

The compositional analysis includes different tests, the total carbonate content, sand fraction, Zr/Rb ratio, and chemical microanalysis. The total carbonate content (%) was determined using a Bernard calcimeter (Alonso et al., 1996). The sand fraction (> 63 μm) composition was analysed by a binocular microscope. Geochemical analysis was performed along core 7 with an Avaatech X-ray fluorescence (XRF) core scanner operated at both 10 kV and 30 kV and with a 1 cm sampling interval at Barcelona University. The Zr/Rb ratio is used as a palaeobottom current intensity proxy because Zr is mainly hosted in heavy minerals of coarse-grained siliciclastic sediments and Rb in fine-grained siliciclastic sediments (Rothwell and Croudace, 2015). SEM morphological observations and semiquantitative chemical microanalysis using SEM Hitachi S-3500 N and SEM-Bruker XFlax 6/30, respectively, were performed on a few glaucony grains collected from distinct sediment layers of cores 8 and 10. Quantax analysis software was used for semiquantitative chemical analysis. The term glaucony used here refers to greenish grains that belong to the glauconite mineral family (Odin and Matter, 1981).

3.6. Seismic profiles

Three seismic profiles (a, b, and c in Fig. 1B) were selected from the database from the Instituto de Ciencias del Mar, ICM-CSIC, http://www.icm.csic.es/geo/gma/SurveyMaps. They have been used to image the different contourite features (terrace T1 and drifts D1 to D4) previously defined in the literature and which have been studied here with sediment cores. For more details about the previous morphoseismic characterization of those contourites features, see Ercilla et al. (2016) and Yenes et al. (2021).

4. Results

4.1. Modern hydrography

The Chullera record, located close to the Strait of Gibraltar, detects a strong current (often surpassing 30 cm/s and reaching up to 47 cm/s) heading southwards towards the Strait (Fig. 2B). This current is opposed at the surface by a current heading northward reaching up to 30 cm/s (Fig. S1). The ranges of temperature and salinity point to MW masses flowing southwards towards the Strait of Gibraltar and to partially mixed AW that originates from the Strait of Gibraltar and heads northwards (Fig. S1). This record shows evidence of semidiurnal variations in speed, temperature and salinity, compatible with the tidal influence that the Alboran Sea experiences on its western side, affected by being in the vicinity of the Strait of Gibraltar. On the other hand, the Marbella record shows much weaker currents on average, mostly below 30 cm/s and rarely surpassing this threshold (Fig. 2C). The current often experiences variations in its direction, mostly heading northwards and southwards (Figs. 2C and S2). This record also shows clear evidence of internal tides in the data recorded during February with the instrument switching from a middle-depth water temperature and salinity to surface temperature and salinity signals (Fig. 2C).

Although the Chullera record shows faster velocities than the Marbella record (Fig. 2B and C), both show velocities within the range above which contourite deposits typically occur (above 15 cm/s) (Stow et al., 2009). Although these records are between 70 and 100 m above the seafloor they allow us to infer that (1) the velocities above the seabed are faster close to the Strait of Gibraltar; (2) these velocities possibly remain

above 15 cm/s, flowing in solidarity with the flow at 70–100 m in the water column; and (3) the internal waves can influence continental slope terrace T1.

4.2. Age model and stratigraphy

The age model of core 7 spans the last 29.5 kyr (Fig. 3A). This age model is consistent with the $\delta^{18}O$ curve from the nearby core C8 (Fig. 3B; Ausín et al., 2015), displaying a good resemblance between $\delta^{18}O$ records. The $\delta^{18}O$ values of cores 7 and C8 reveal high-quality and continuous records documenting the existence of high-amplitude and high-frequency variability over the last glaciation and Holocene interglacial, allowing us to recognize six climatic periods: Heinrich Stadial 3 (HS3), Heinrich Stadial 2 (HS2), Last Glacial Maximum (LGM), Heinrich Stadial 1 (HS1), Younger Dryas (YD) and Holocene (Fig. 3). According to the generated age model, the linear sedimentation rate of core 7 ranges from 7 to 22.8 cm/kyr (Fig. 3C) with an average of 16 cm/kyr, and the sampling resolution is centennial (156 years) for the applied sampling between 2 and 3 cm intervals. The linear sedimentation rate of core C8 varies from 11 to 80 cm/kyr (Fig. 3D) with an average of 36.9 cm/kyr, and the sampling resolution is 68 years.

The chronology of the other cores enables recognition of the following climate periods (Fig. 4): HS1 (in core 2), YD (in cores 1, 2, 5 and 12) and Holocene (in all cores). The ages obtained by AMS ^{14}C analysis in the upper part of cores 8 and 10 vary from 3.8 and 2.1 kyr, leading to low sedimentation rates of 7.9 and 9.5 cm/kyr, respectively (Fig. 4). The bottoms of cores 5 and 11 have ages of 12.1 and 11.7 kyr, respectively, resulting in sedimentation rates of 23 and 10.5 cm/kyr, respectively (Fig. 4). We note that the position of YD of core 12 is based on the similar Ca curve of near core 7 whose age model is supported by the oxygen-isotope curve.

4.3. Sedimentary facies and sequences

4.3.1. Descriptive and interpretative facies

Eight facies named F1 to F8 are identified based on texture, median grain size (D50), sorting, sand fraction composition, carbonate content and sedimentary structures (Figs. 5, 6 and 7). Detailed sedimentological characteristics of facies are illustrated in Table 3. Each facies is briefly described as follows. *Facies F1* consists of mixed (terrigenous-biogenous components) homogeneous muds and represents the finest-grained sediments; *facies F2* consists of mixed mottled silty sediments with frequent bioturbation; *facies F3* consists of bioturbated sandy silt; and *facies F4* corresponds to mixed bioturbated silty sand and sand sediments representing the coarsest sediment (Fig. 6A and B). The mixed components of facies F1, F2, F3 and F4 are mostly formed by benthonic and planktonic foraminifera as biogenic components and quartz as a terrigenous component (Fig. 7A), with the exception of the shallow cores on terrace T1, which also contain abundant glaucony grains and fragments of gastropods and bivalves (Fig. 7B); *facies F5, F6 and F7* comprise terrigenous silty sand (F5), sandy silt (F6) and silty sediments (F7), respectively, with abundant angular and subangular quartz (Fig. 7C); and *facies F8* consists of mixed silty sediments with subangular and rounded quartz, rock fragments, benthonic and planktonic foraminifera, as well as fragments of bivalves and gastropods (Fig. 7D).

The glaucony grains are mainly infilled moulds of foraminifera tests. They are characterized by ovaloid, lobulated and rounded green, dark green to black grains (Fig. 7E, F and G) with variable proportions of

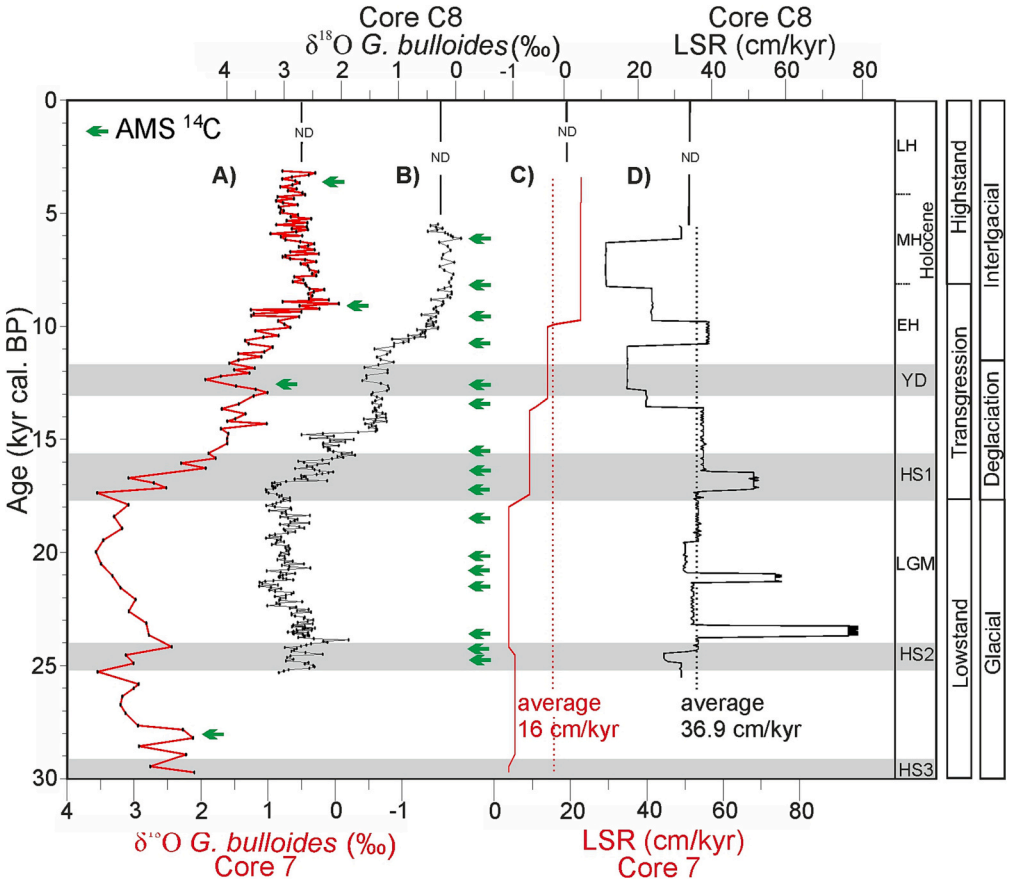

Fig. 3. Chronologic framework for cores 7 and C8. (A and B) Planktonic oxygen isotopic records of cores 7 and C8, respectively. (C and D) Linear sedimentation rate (LSR) of sediment cores 7 and C8, respectively. The grey bars indicate cold stadials (HS3 Heinrich Stadial 3, HS2 Heinrich Stadial 2, HS1 Heinrich Stadial 1, and YD Younger Dryas). LGM Last Glacial Maximum. EH Early Holocene., MH Middle Holocene. LH Late Holocene. ND No data.

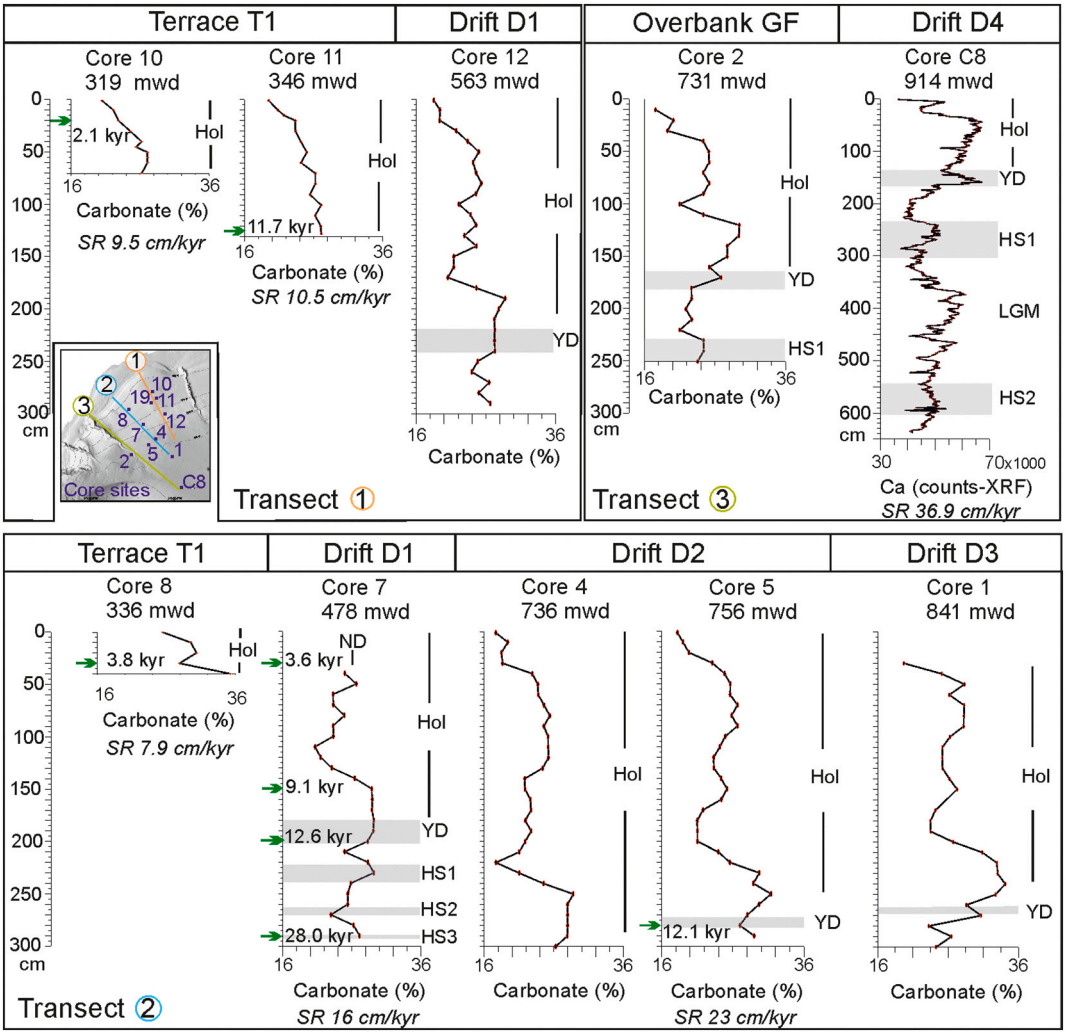

Fig. 4. Stratigraphy of the sediment cores based on facies, carbonate content, Ca (count-XRF), AMS ^{14}C data and age model of cores 7 and C8. The grey bars indicate cold stadials (HS3 Heinrich Stadial 3, HS2 Heinrich Stadial 2, HS1 Heinrich Stadial 1, and YD Younger Dryas). Legend: LGM Last Glacial Maximum; Hol Holocene; GF Guadiaro Fan; SR Sedimentation rate; mwd metres water depth.

cracks (Fig. 7H and I). Some grains have shiny surfaces under a binocular microscope (Fig. 7F) and lamellar and "rosette" microstructures under SEM (Fig. 7J and K). Chemically, the glaucony grains are characterized by high contents of SiO_2, FeO and K_2O, with black grains enriched in FeO and K_2O (Fig. 7L).

Facies F1 to F4 are interpreted as contourite sediments based on the main sedimentological diagnostic criteria described by Faugères et al. (1984), Stow and Faugères (2008), Stow et al. (1986), and Alonso et al. (2021) that involve coarsening-fining upward sequences, bioturbation (Fig. 6A and B) and mixed composition (Fig. 7A). Thus, facies F1 to F4 belong to the classical C1 to C5 divisions. The homogenous mud facies (F1) belong to C1/C5; the mottled silty facies (F2) equates to C2/C4; and the sandy silt facies (F3) and silty sand and sand facies (F4) correspond to the C3. F3 and F4 represent the silt/sand-rich part of the succession and they show variations in texture. These variations allow us to subdivide C3 into C3a, C3b, and C3c, which correspond to facies F3, F4 and F3, respectively (Fig. 6A). C3a and C3c contain up to 64% silt and 28% sand and comprise coarse to very coarse silt in cores 7, 8, 11, 12, and C8 (Figs. 5 and 9; Table 3). C3b contains up to 52% sand and 42% silt in cores 2, 7, 8, 10, 11, and up to 80% sand in core C8 (Figs. 5 and 11B). The dominant texture is very coarse silt to fine sand (Table 3). Theses oscillations in grain size within C division have been also recognized recently by Stow et al. (2023).

The terrigenous facies F5, F6 and F7 are interpreted as turbidites based on the main sedimentological diagnostic criteria described by Bouma (1962). Facies F5, F6 and F7 are equivalent to the Tb, Tc and Td divisions of Bouma's (1962) sequence, respectively (Fig. 6C). The following characteristics are common to turbidites, and they allow their distinction from contourites (Figs. 6C and 7C): (i) terrigenous composition with abundant angular and subangular quartz grains and with layers rich in organic matter; (iii) sharp bases and gradational tops; (iv) fining-upwards sequence (Tb-Tc-Td and Tc-Td); and (iv) parallel (Tb) and cross lamination (Tc).

Facies F8 beds show erosional bottom surface, attenuated lamination, bioturbation, sharp upper contact (Fig. 6D), and mixed sand fraction composition. F8 is interpreted as contourite/turbidite mixed sediments (Fig. 7D) in agreement with Mulder et al. (2008).

4.3.2. *Sequences of facies*

The stratigraphic arrangement of the above facies allows us to define ten sequences, which are named S1 to S10 (Fig. 8). The sequences S1 to S7 correspond to contourites that are grouped into four types according to the classification of Stow and Faugères (2008) (Fig. 8A): (i) partial bigradational, (ii) coarsening-upwards, (iii) fining-upwards, and (iv) homogenous. The partial bigradational contourite sequence (i) shows coarsening-upwards to fining-upwards grain-size distribution and comprises sequences S1 (C2-C3a-C2), S2 (C1-C2-C1) and S3 (C2-C3a-C3b-C3c-C4). The coarsening-upwards sequence (ii) includes S4 (C1–C2-C3a-

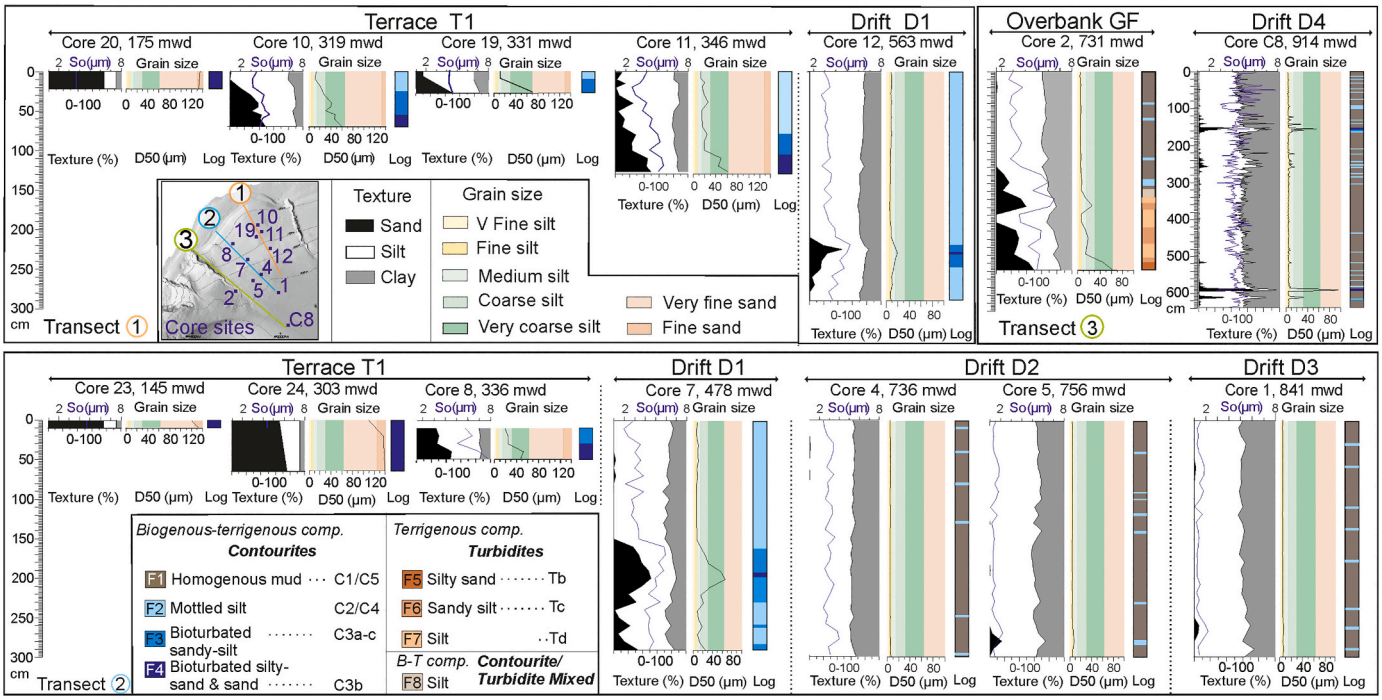

Fig. 5. Sedimentary facies (descriptive and interpretative) characterizing contourite terrace T1, contourite drifts D1 to D4, and the overbank of the Guadiaro Fan (GF). The sedimentological characteristics defining their facies are illustrated along three transects (1 to 3); from left to right: texture (%), sorting (So μm), median grain size (D50 μm), and log facies. Notice the different scale of D50 for the cores of terrace T1 and the different vertical scale of core C8. Legend: mwd metres water depth; B-T Biogenous-Terrigenous; Comp Composition.

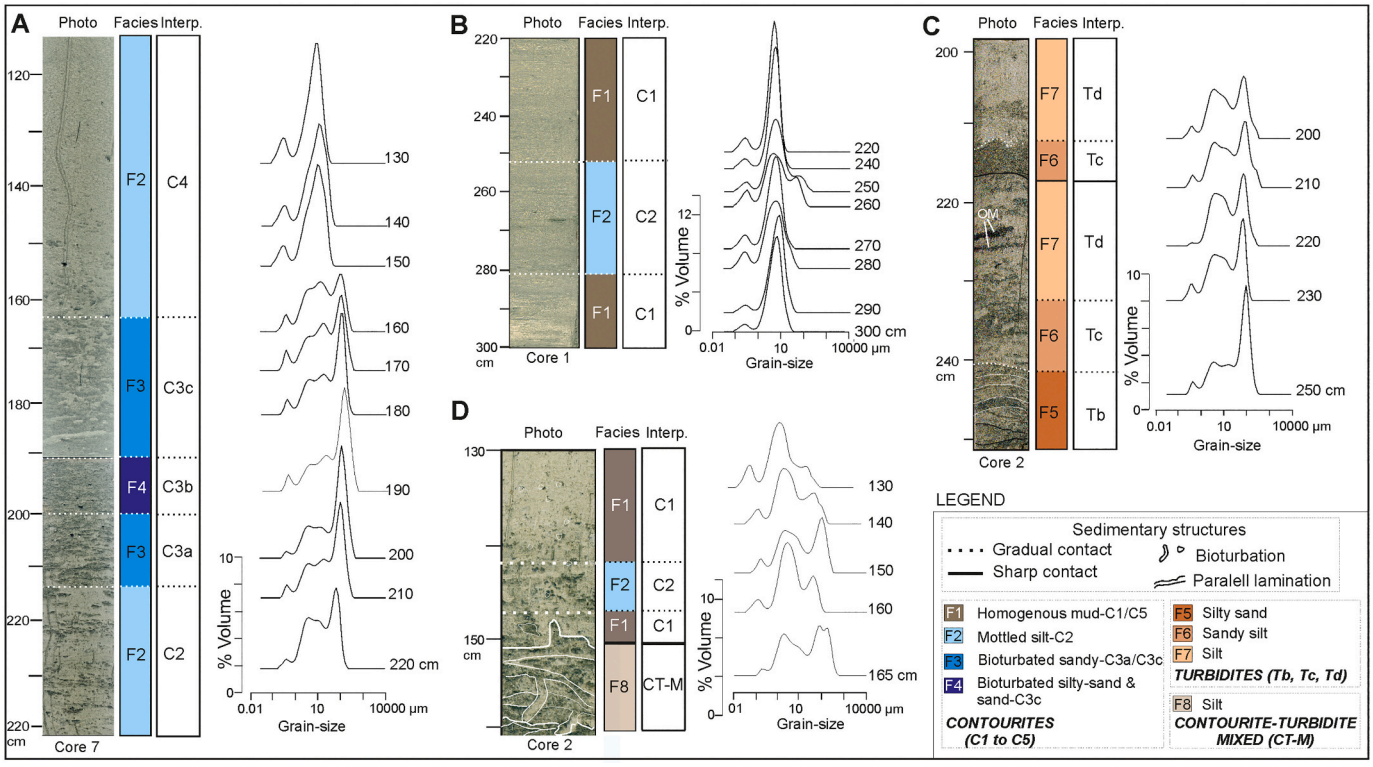

Fig. 6. Visual features and grain-size distribution of facies. From left to right: core photo, facies (F1 to F8), interpretative facies (contourite, turbidite and contourite/turbidite mixed), and vertical distribution of grain size distribution for selected intervals of cores 1, 2 and 7. Legend: Inter Interpretation; OM Organic matter.

C3b), which represents the topcut-out contourite sequence. The fining-upwards sequence (iii) is formed by S5 (C3b-C3c-C4) and S6 (C3c-C4-C5), which represent the basecut-out sequence. The homogenous sequence (iv) is formed by S7 (C3b). It is important to note that S5 may correspond to an incomplete sequence because the presence of coarse grain sizes at the bottom of cores 8, 9 and 10 could inhibit the

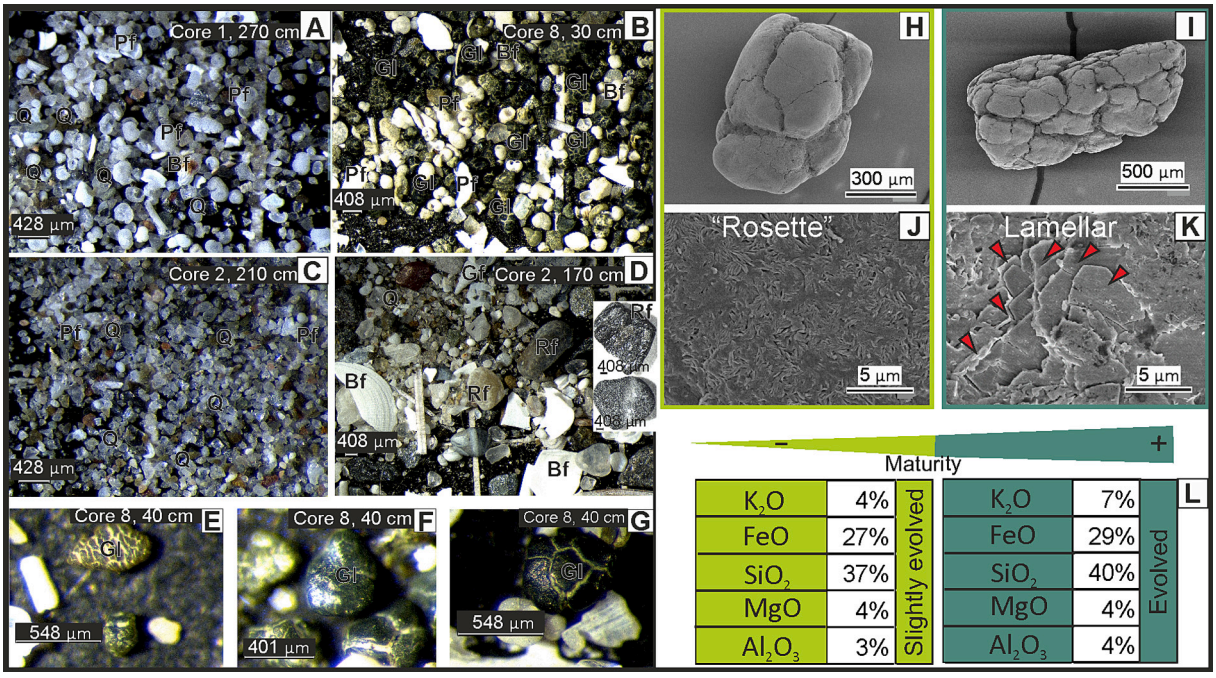

Fig. 7. Sand fraction composition of facies and characteristics (morphology, colour and chemical composition) of glaucony grains. (A-G) Binocular microscope photos of the sand fraction showing: (A) Mixed composition with foraminifera (entire and fragments) and quartz of contourites from drifts D1 to D4; (B) Mixed composition with glaucony grains of contourites from terrace T1; (C) Terrigenous composition with quartz and rock fragments of turbidites from the overbank of Guadiaro Fan. (D) Mixed composition with gastropods and bivalve fragments, rounded rock fragments of contourites/turbidite mixed sediments from the overbank of Guadiaro Fan. (E-G) Detail of glaucony grains showing green and darker green colours with crack (E) and polished (F) surface. (H-K) SEM microphotograph of glaucony grains displaying the external shape in H and I with cracks and internal nanostructures (i.e., "rosette" and lamellar structures in J and K). (L) Chemical microanalysis measured on green and darker green glaucony grains. Legend: Q quartz; Pf planktonic foraminifera; Bf benthonic foraminifera; G glaucony; Gf gastropoda fragments; Rf rock fragments. (For interpretation of the references to colour in this figure legend, the reader is referred to the web version of this article.)

Table 3
Summary of the main sedimentological characteristics of facies (F1 to F8). Facies F1 to F4 are contourites equivalent to the C1 to C5 divisions, facies F5, F6 and F7 correspond to the Tb, Tc and Td turbidite divisions, and facies F8 is a contourite/turbidite mixed facies.

Facies	Interp	Texture	D50 (micres)	Sorting	Composition		Visual observation	
					Dominantly	Carbonate (%)	Contacts	Structures
F1	C1/C5	Mud with <10% sand	Very fine to fine silt	Well to poorly sorted	B-T: Forams, shelf fragments, quartz	Moderate to high (up to 30)	Gradual BS & US	Moderate biot
F2	C2/C4	Silt (up to 86%)	Fine to coarse silt	Well to very poorly sorted	B-T: Forams, shelf fragments, quartz	Moderate to high (up to 30)	Gradual BS & US	Moderate biot
F3	C3a/ C3c	Sandy silt with <30% clay	Coarse to very coarse silt	Very poorly sorted	B-T: Forams, shelf fragments, quartz	Moderate to high (up to 30)	Gradual BS & US	High biot
F4	C3b	Silty sand with <15 clay	Very coarse silt to fine sand	Poorly to very poorly sorted	B-T: Forams, shelf fragments, quartz	High (up to 35)	Gradual BS & US	High biot
F5	Tb	Silty sand with <24% clay	Medium silt to very fine sand	Poorly to very poorly sorted	T: Angular & subangular quartz	Moderate (<20)	Sharp BS, Gradual US	Parallel lamin
F6	Tc	Sandy silt wiht <33% clay	Fine to to medium silt	Very poorly sorted	T: Angular & subangular quartz	Moderate (<23)	Gradual BS & US	Cross lamin, Organic matter
F7	Td	Silt (up to 70% silt)	Fine to to medium silt	Very poorly sorted	T: Angular & subangular quartz	Moderate (⟨23)	Gradual BS, Sharp US	Parallel lamin
F8	CT-mixed	Sandy silt with <32% clay	Fine to to medium silt	Very poorly sorted	B-T: bivalves & gastropods frag, forams, quartz, rock frag	Moderate (< 28)	Erosional US & BS	High biot Attenuated lamin

Legend: B Biogenous; T Terrigenous; frag fragments; BS Basal surface; US Upper surface; biot Bioturbation; Lamin Lamination; Interp Interpretation.

penetration of the sampling device gear. The spatial distribution of these contourite sequences is described as follows (Figs. 9 and 10): (i) on contourite terrace T1, the fining-upwards sequence S5 and the homogeneous sequence S7 are dominant; (ii) on drift D1, the bigradational sequences S1 and S3 prevail; and (iii) on drifts D2 to D4, the bigradational sequence S2 is dominant with minor occurrence of sequences S4, S6 and S7.

S8 and S9 represent turbidite sequences that make up the fining-upwards sequence and comprise the Tb-Tc-Td (S8) and Tc-Td (S9) divisions (Fig. 8B). The contourite/turbidite mixed facies forms sequence S10 (Fig. 8C). These three sequences (S8, S9, and S10) are on the overbank area of the Guadiaro Fan (core 2 in Fig. 9C).

4.4. Physical and chemical proxies for bottom current strength

Physical (e.g., sand content, D50, and UP10 percentage of the non-carbonated fraction) and chemical proxies (Zr/Rb ratio) of palaeobottom current intensity were examined in cores 7 and C8 (Figs. 11 and 12) for the last 29.5 kyr. The physical proxies display similar temporal patterns in both cores, showing overall high peaks at HS3, HS2, HS1 and

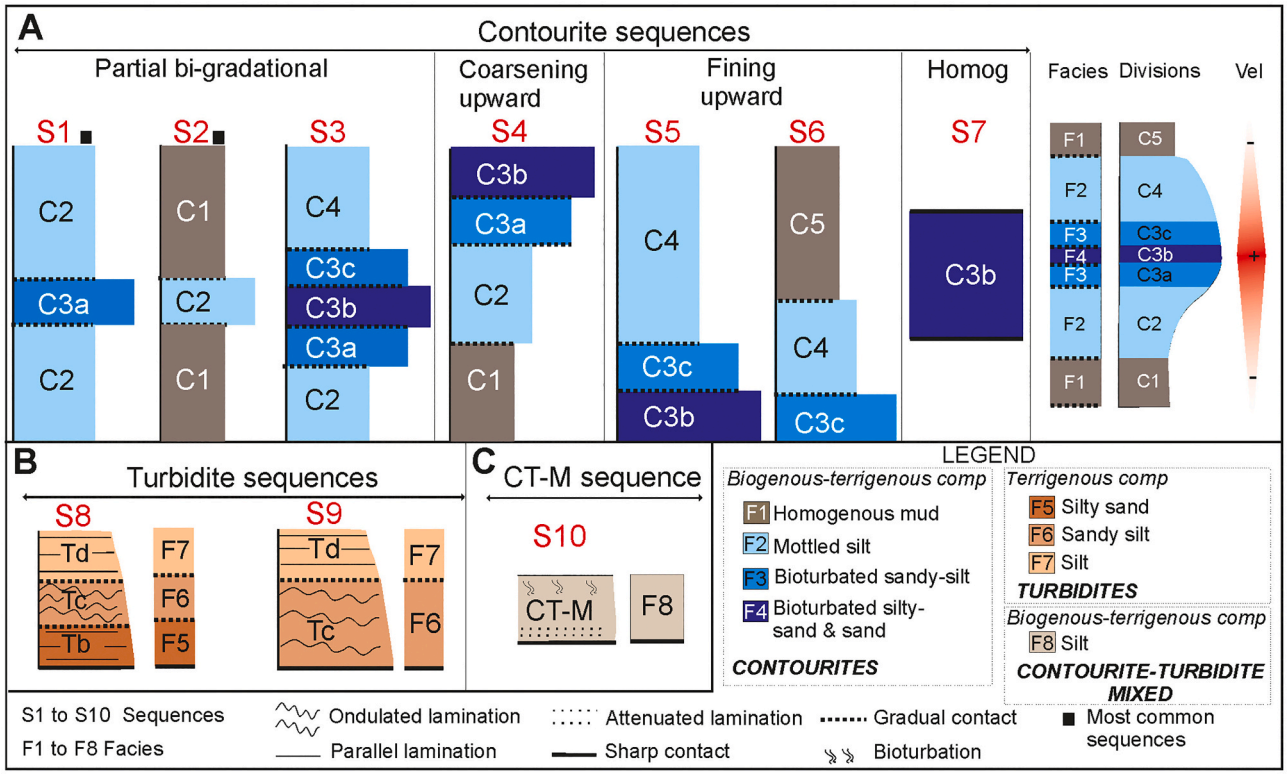

Fig. 8. Representation of the facies sequences (S1 to S10). (A) Contourite sequences (S1 to S7) that show variations on the standard contourite model of Stow and Faugères (2008); the proposed subdivisions C3a, C3b, C3c within the C division are also shown. (B) Turbidite sequences S8 interpreted as Tb, Tc and Td divisions and S9 formed by Tc and Td divisions of Bouma sequence (Bouma, 1962). (C) Contourite/turbidite mixed sequence (CT-M; S10) formed by facies 8. Legend: Vel velocity of bottom current; Comp Composition; Homog Homogenous.

YD (Fig. 11). These peaks match the maximum peaks of the Zr/Rb ratio (Fig. 11). The UP10 record of core 7 displays 30 peaks (named A1s-A41s; A = Alboran, s = slope), and core C8 shows 30 peaks (named A5b-A38b; b = basin) that are ordered from younger to older and represent fast current events (FCE in Fig. 12B and C). The number indicates age, so equal numbers imply contemporary FCE at both cores (e.g., A19s and A19b at YD; Fig. 12B and C), most of which coincide with relatively high values in $\delta^{18}O$ (Fig. 12A). The highest distinct FCE in both cores is found for the YD (Fig. 12). The cyclicity of the FCE on drift D1 (core 7 in Fig. 12B) ranges from 1.3 kyr to 0.6 kyr, and that on drift D4 (core C8 in Fig. 12C) ranges from 0.8 to 0.5 kyr.

5. Discussion

5.1. Contourite stratigraphic models: Sedimentary signals of palaeocurrent strength and palaeoclimate significance

Two contourite stratigraphic models, terrace and drift, are established in the Alboran Sea based on the stratigraphy of sequences that form the modern terrace T1 and drifts D1 to D4 across the upper slope to the basin (Figs. 9, 13 and 14). The sedimentological data of contourite sequence types (S1 to S7) are well grouped in the binary diagram sorting versus D50 (Fig. 10), allowing the identification of these models as well as the differentiation of the bottom water masses (Fig. 13).

5.1.1. Contourite terrace model: An archive of the bottom current and glacioeustasy interplay

This model is defined by the coarse-grained sediments rich in glauconi that involve a homogenous sequence S7 (C3b) in the shallow domain (± 145 to 303 mwd) and a fining-upwards sequence S5 (C3c-C3b-C4) in the deeper domain (± up to 346 mwd) (Figs. 9A, 13 and 14). On both domains, the top sediments of sequences form an alongslope regional sheet of relatively coarser sediments that become finer down terrace, from sandier to siltier (Fig. 9A). Previous studies based on seismic records suggested that the erosive character of contourite terrace T1 (a truncating high reflectivity surface) is related to turbulent oceanographic processes (internal waves) associated with shifts in the AW-LMW interface during the Quaternary glacioeustasy (Fig. 14; Ercilla et al., 2016; Juan et al., 2020). Although the time span of most geological processes does not match most oceanographic physical processes (Rebesco et al., 2008), the studied current meters also confirm the occurrence of internal waves on terrace T1 (Fig. 2C). Their turbulent oceanographic action impinging on the seafloor would have favoured sediment resuspension and lateral transport (Juan et al., 2020). The new sedimentological results also confirm the emplacement of coarse-grained sequences S5 and S7 in an energetic environment (Fig. 14). Bottom current velocities >23 cm/s could be tentatively attributed to the deposition of sequence S5, and up to 36 cm/s for sequence S7, based on estimated palaeo-velocities of similar contourite sequences by Alonso et al. (2021) in the Alboran Sea. The presence of silt and sand requires velocities of over 30 cm/s (McCave, 2008; Van Rooij et al., 2007). Furthermore, the studied current meters registered velocities up to 50 cm/s (Chullera record) and 45 cm/s (Marbella record) (Fig. 2B and C). One consequence of these high velocities on sediment transport is the lateral winnowing of clay particles, a process considered to be the primary mechanism for explaining the lack of muddy sediments (C1) in sequences S5 (C3b-C3c-C4) and S7 (C3b) (Fig. 13). The sedimentological characteristics distinguishing the contourite terrace model are in overall agreement with sedimentary results on other contourite terraces, such as on the Demerara Plateau (Tallobre et al., 2016), the La Plata terrace (Preu et al., 2013), and the Piedra Buena terrace (Isola et al., 2021).

It has been widely proposed that the seaward and landward shifts of the coastline by Quaternary glacioeustatic sea-level changes have conditioned the spatial and temporal distribution and composition of

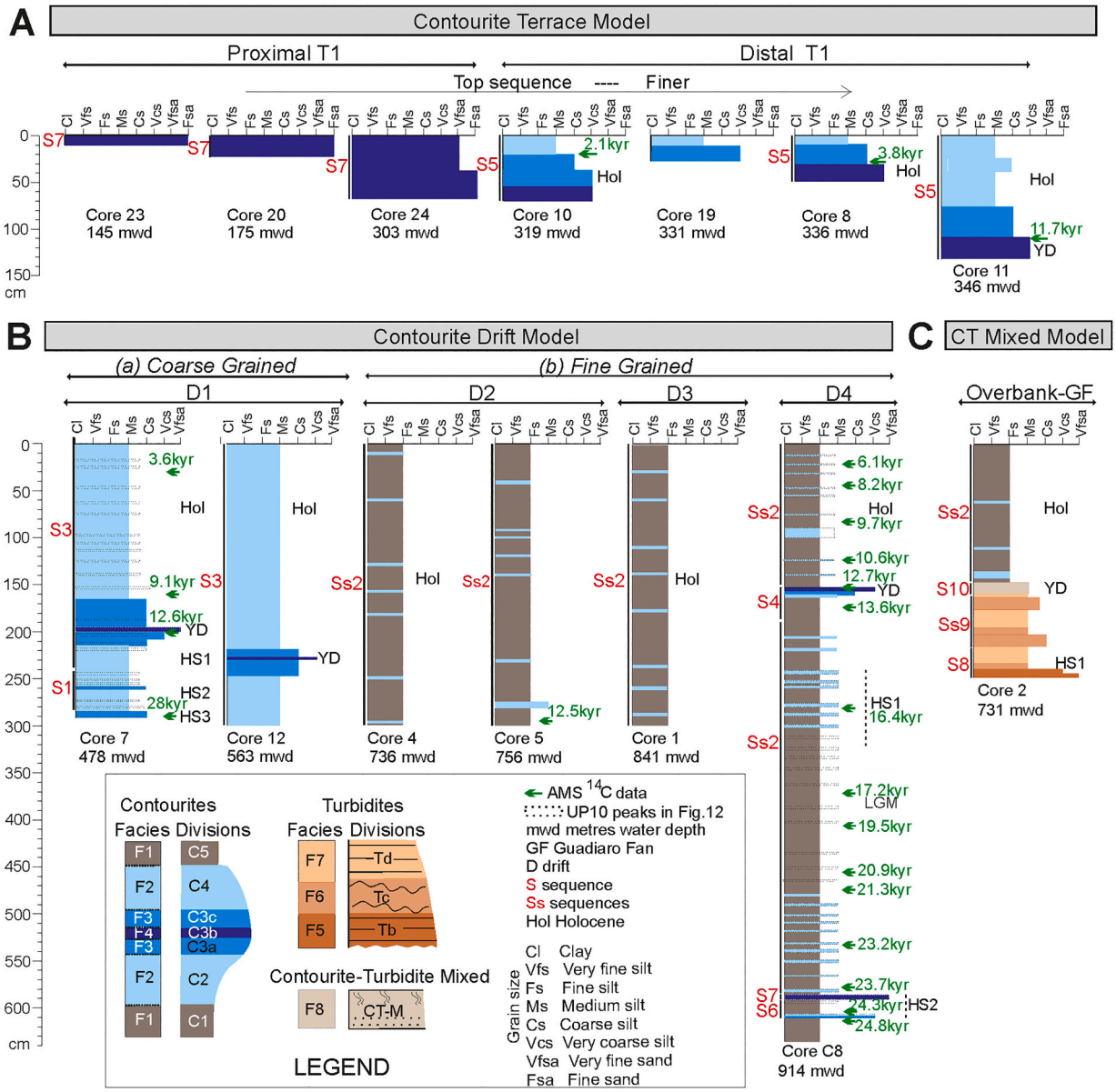

Fig. 9. Contourite stratigraphic models: (A) Contourite terrace model; (B) Contourite drift models (coarser and finer-grained); and (C) Contourite/turbidite mixed model. Named facies in Fig. 5. Legend: HS3 Heinrich Stadial 3; HS2 Heinrich Stadial 2; LGM Last Glacial Maximum; HS1 Heinrich Stadial 1; YD Younger Dryas; Hol Holocene; CT-M Contourite/turbidite mixed; mwd metres water depth.

sediments on continental slopes due to inland sediment supply variations (e.g., Chiocci et al., 1997; Ercilla et al., 2022; Lobo et al., 2014). However, the above interpretation for the terrace model suggests that its sequence stratigraphy could also reflect the interplay of sediment supply variations with the shallowing of the AW-LMW interface. That shallowing would occur during the Versilian postglacial transgression (onset of the YD to onset of the middle Holocene) (Fig. 14). This sea-level variation would have provoked vertical and lateral displacements of the AW-LMW interface and the associated energetic oceanographic processes (e.g., internal waves). Several lines of evidence support this interpretation. (i) The age of the top silts of sequence S5 is 2.1 kyr (core 10 in Fig. 9A) and that of the nearby bottom silty sands is 11.7 kyr (end of YD; core 11 in Fig. 9A); then, sequences S5 and S7 formed at least during the Latest Pleistocene (YD) and mostly during the Holocene (Fig. 14). (ii) The presence of fragments of bivalves and gastropods in the sand fraction of sequences S5 and S7 indicates that they were sourced from the adjacent outer continental shelf by shelf-spill-over processes due to shelf currents and/or storms during the Versilian transgression (Ercilla et al., 1994; Stanley et al., 1972). The transport of fragments would have been affected by the circulation being deposited with a dominant alongslope component (Ercilla et al., 2016; Preu et al., 2013; Viana, 2007). (iii) The fining upwards trend of sequence S5 (C3b-C3c-C4; from sandier to siltier sediments; Figs. 13 and 14) would be also related to the shallowing of the interface during the transgression, which also led to its horizontal-landward migration. This fact would have provoked a decrease in the action of turbulent oceanographic processes in the deeper terrace with time, favouring the vertical change from sandier to siltier deposits (Fig. 9A). Likewise, the interface shallowing would explain the deposition of the massive sands comprising sequence S7 in the proximal terrace domain (Fig. 9A) since the AW-LMW interface settled there during the highstand position of sea level (Fig. 14). This landward migration of the interface would also explain the fining seaward trend of the surface contourite terrace sediments from sandier to siltier (Fig. 9A).

Regarding the glaucony grains, large amounts of these particles characterize the sand fraction of sediments (Fig. 7B), making up

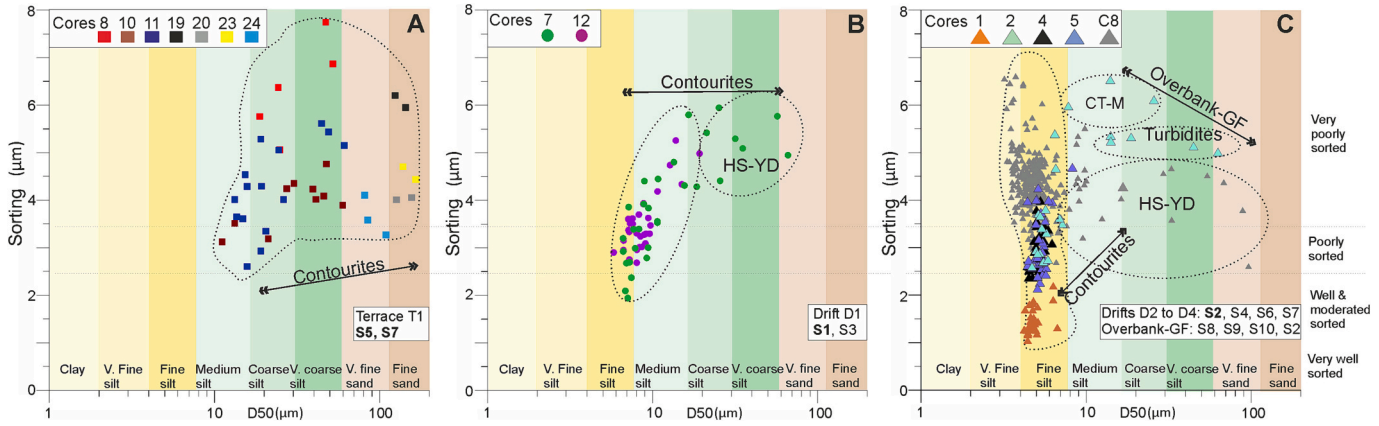

Fig. 10. Binary textural plots of sorting versus D50 of contourite, turbidite and contourite/turbidite mixed sequences. (A) Contourite sequences S5 and S7 of terrace T1. (B) Contourite sequences S1 and S3 of drift D1. (C) Contourite sequences S2, S4, S6 and S7 of drifts D2, D3 and D4, turbidite sequences S8 and S9 and contourite/turbidite mixed S10 (CT-M), and contourite S2 of the overbank Guadiaro Fan (GF). The bold name of the sequence refers to the dominant sequence. Legend: V Very; HS Heinrich stadial sediments; YD Younger Dryas sediments.

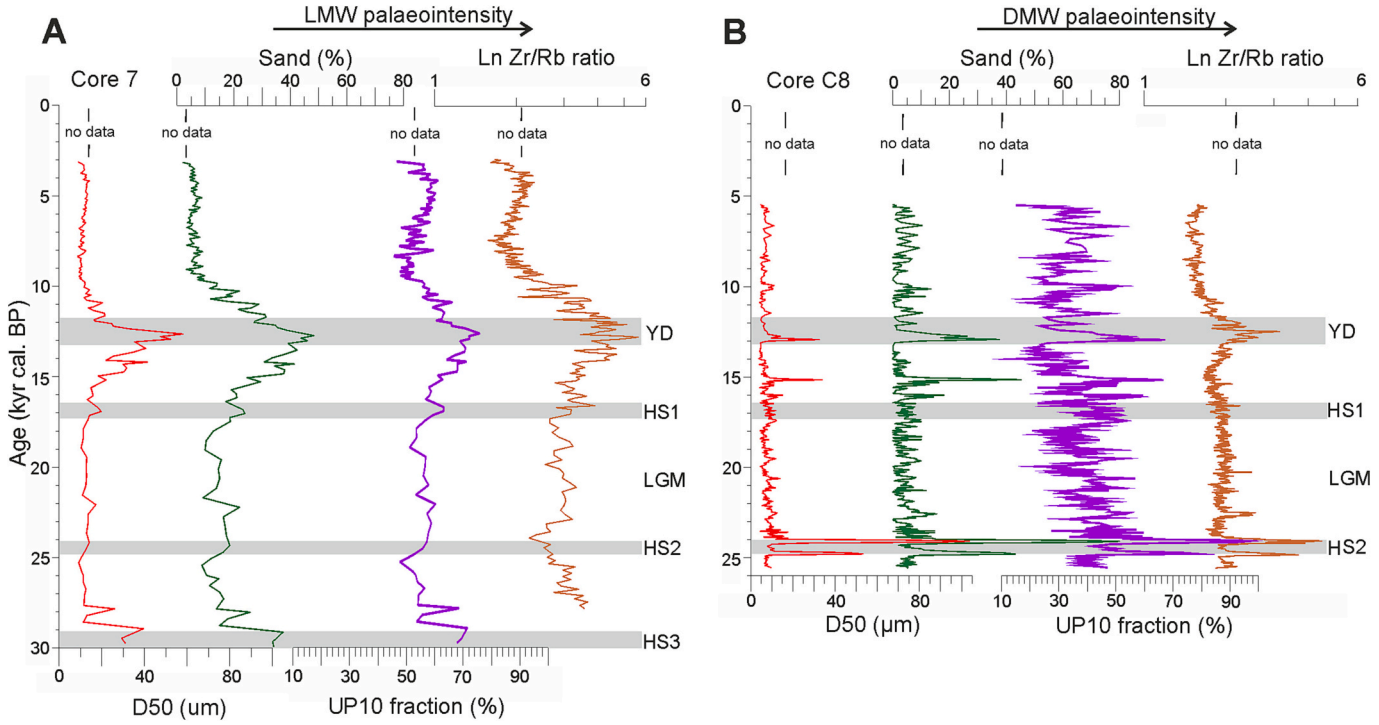

Fig. 11. The 4th-order, millennial and centennial palaeointensity of the light intermediate Mediterranean water (LMW) and Dense Deep Mediterranean water (DMW) for the last 29.5 kyr. The palaeointensity fluctuations are evidenced by the temporal distribution of D50, sand percentage, UP10 percentage of noncarbonate fraction and Zr/Rb ratio in cores 7 (A) and C8 (B). The grey bars indicate cold stadials: Heinrich Stadials (HS3, HS2, HS1) and YD Younger Dryas.

sequences S5 and S7 of the contourite terrace model (Figs. 13 and 14). A common problem encountered in the sedimentary record is truly distinguishing the allochthonous or authochthonous (authigenic) genesis of glaucony (Amorosi, 1996). A review of the contourite terrace literature suggests scenarios with both origins but also mixed origins (Cunningham et al., 2002; Giresse et al., 2021; Tallobre et al., 2016, 2019). A mixed origin has been reported on the Falkland Plateau (eastern Argentina), where glaucony may be produced partly by contemporaneous authigenic formation and partly by erosion of outcropping Cretaceous and Tertiary glauconite-rich strata due to the action of strong bottom currents (Cunningham et al., 2002). The glauconitization process on terrace T1 commonly occurs in filled moulds of foraminifera tests (Fig. 7E, F and G), which provide microreducing environments favourable for this diagenetic process (Giresse, 2008). The results of the chemical composition of glaucony grains reveal different rates of enrichment in K (from 4 to 7% in K_2O; Fig. 7L) and Fe (from 27 to 29% in FeO; Fig. 7L), indicating chemical evidence of the maturation processes (Banerjee et al., 2016; Giresse, 2008; Odin and Fullagar, 1988). Similar values have been reported for glaucony grains found on contourite sequences (i.e., Tallobre et al., 2019). The laminallae and "rosette" microstructures (Fig. 7J and K), the abundance of grains with dark green colour (Fig. 7B), the presence of cracks (Fig. 7H and I) and polished surface (Fig. 7F) are additional indicators of their maturity (Odin and Letolle, 1980; Odin and Matter, 1981). All these evidences allow us to propose that most of the glaucony grains on terrace T1 can be classified as "slightly evolved" and "evolved" types in the evolutionary process of glauconitization, i.e., glauconites in the 2nd and 3rd stages of the four evolutionary stages of the process (Fig. 7L; Amorosi, 1996; Odin and

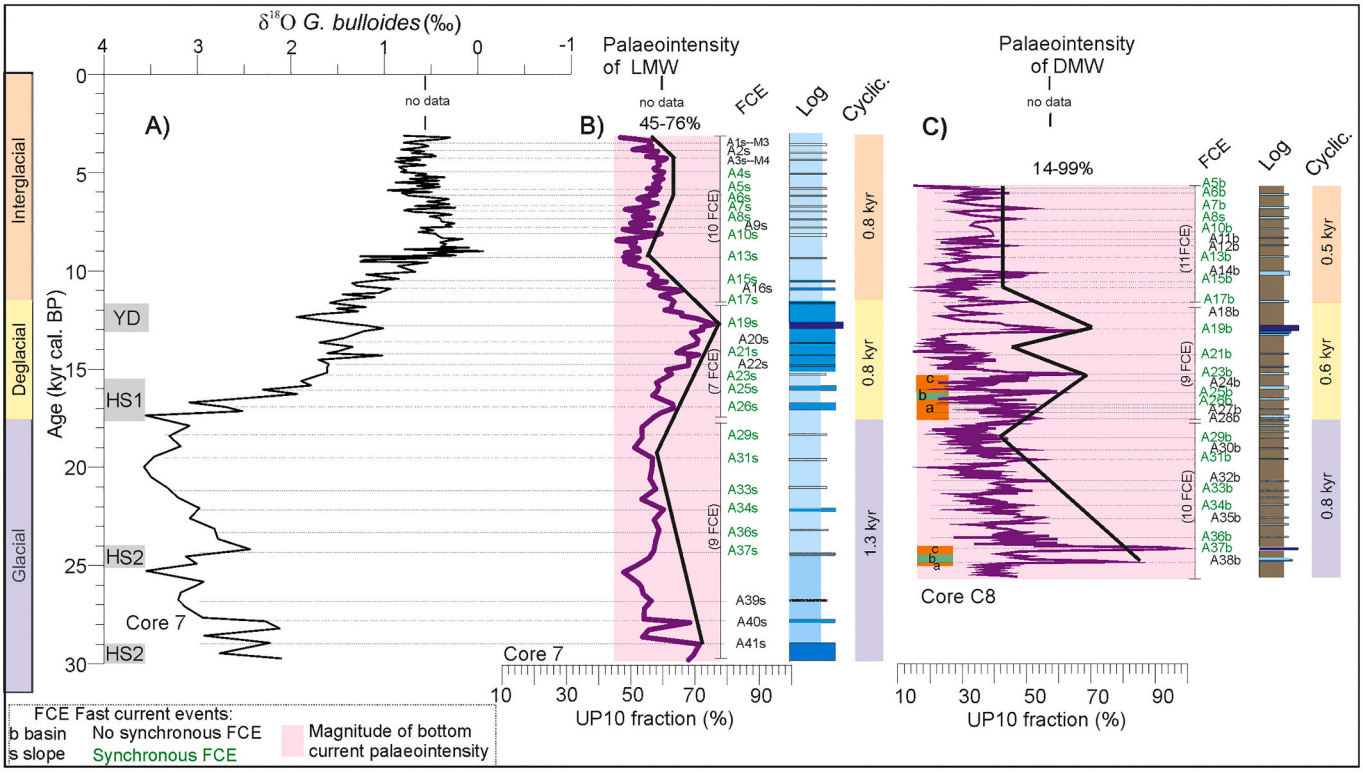

Fig. 12. Correlation between events of enhanced LMW (Light Intermediate Mediterranean water) and DMW (Dense Deep Mediterranean water) intensity at cores 7 and C8 during the last 29.5 kyr. (A) isotope oxygen record of core 7. (B and C) temporal distribution of UP10 of cores 7 and C8 showing fast current events (FCE), cyclicity (cyclic) of these events and facies log. FCE named are from younger to older; A1s to A41s for core 7 and from A5b to 38b for core C8. The grey bars indicate cold stadials: Heinrich Stadials (HS3, HS2, HS1) and YD Younger Dryas; a, b and c phases for HSs. Legend of facies in Fig. 5. Thick lines pattern refers to 4th-order fluctuation of bottom currents.

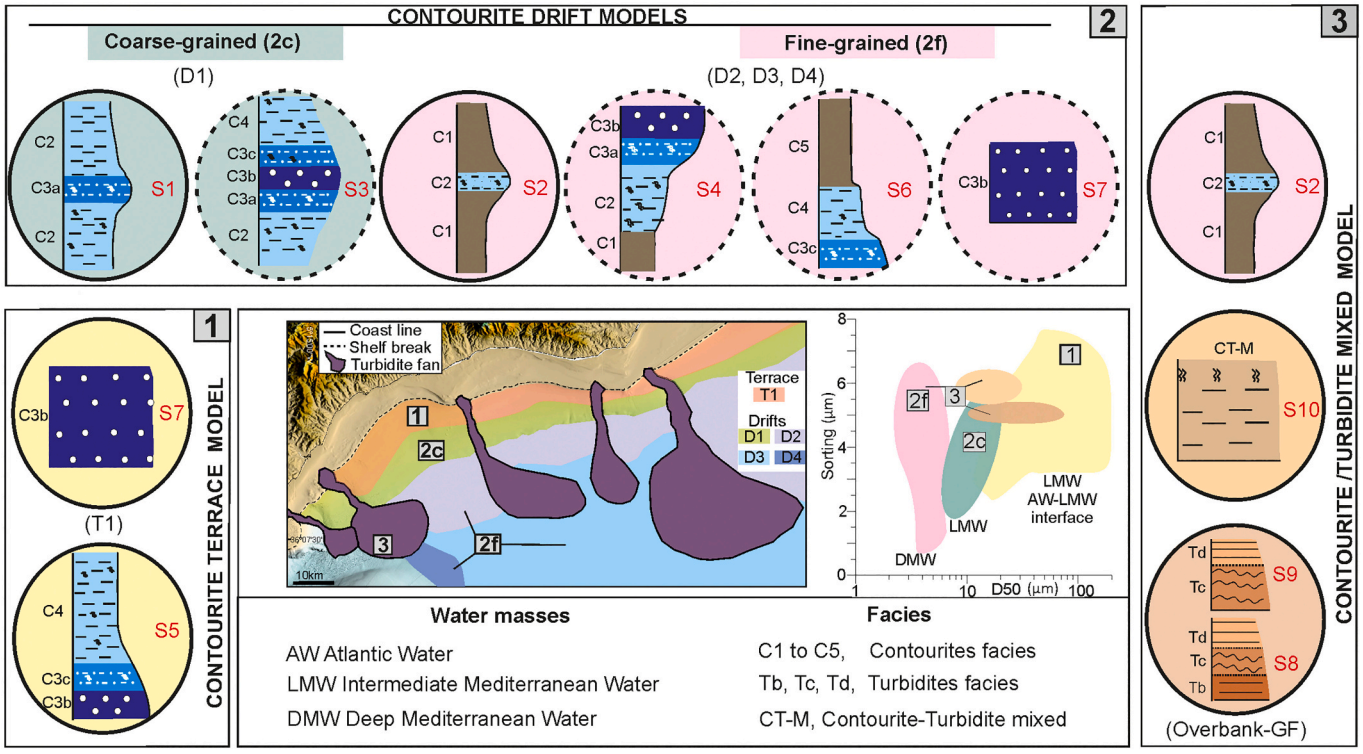

Fig. 13. Summary of the main facies, sequences (S1 to S10) and stratigraphy of sequences defining three sedimentary models for the Alboran Sea: 1 contourite terrace model, 2 contourite drift models (coarse-2c and fine-grained-2f) and 3 contourite/turbidite mixed model. Colours differentiating the stratigraphic log models refer to different water masses and match those in the binary textural plot D50 versus sorting (for more details, see Fig. 10). Legend of facies in Fig. 5.

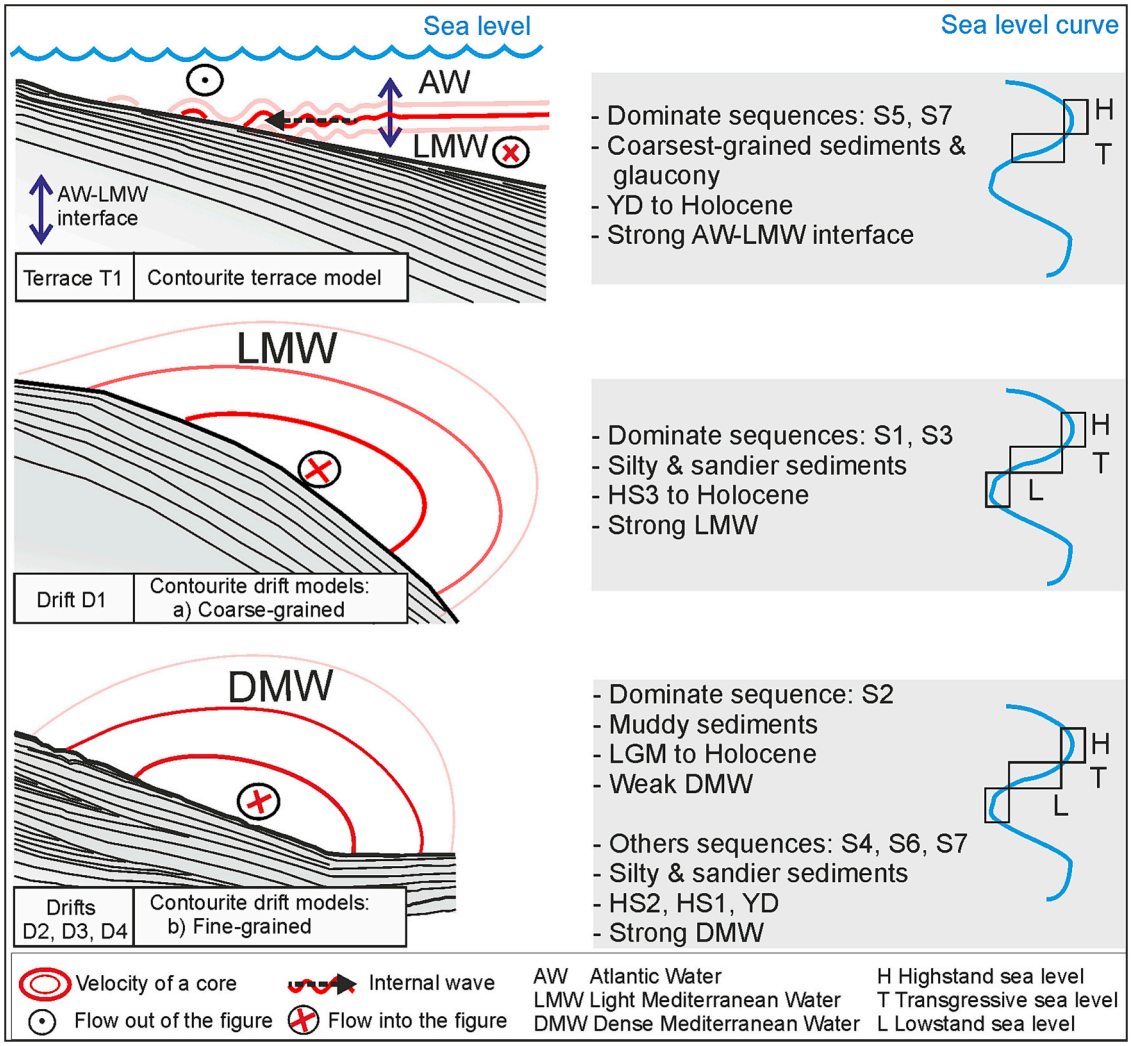

Fig. 14. Three cartoons showing the relationship between the alongslope bottom currents, the contourite terrace T1 and drifts (D1 to D4) (based on Juan et al., 2020), and their dominant sediments and sequences formed during the different stages of the sea level curve variation (highstand, transgressive, and lowstand). Legend: HS1, HS2, HS3 Heinrich Stadials; YD Younger Dryas.

Matter, 1981).

In agreement with other marine sequences (Banerjee et al., 2016; Eder et al., 2007; Giresse, 2008), the environmental conditions require low sedimentation rates for the glauconitization process, and in the study case, they are closely associated with energetic bottom currents that favour winnowing. The turbulent processes associated with the AW-LMW interface create energetic hydrodynamic (bottom currents up to 50 cm/s) and sedimentary conditions (low sedimentation rate <10 cm/kyr). These conditions would have favoured the neoformation of glauconi at terrace T1 during the last postglacial transgression. Furthermore, their maturity allows us to consider their prolonged exposure at the water-sediment interface mainly during the end of the transgression and highstand because mineral evolution requires cation exchange over long periods (Giresse, 2008). The presence of glauconi grains through sequences S5 and S7 confirms the persistent occurrence of those conditions during the latest Pleistocene-Holocene on terrace T1 (Fig. 14).

5.1.2. *Contourite drift models: Archives of rapid ocean-climate coupled fluctuations*

The contourite drift models comprise two stratigraphies of sequences: i) one coarser (Figs.13 and 14) for the shallower drift D1 (478–563 mwd) and ii) another finer (Figs.13 and 14) for the deeper drifts D2, D3 and D4 (731–914 mwd; Fig. 9B).

(i) The coarse-grained drift model involves the bigradational sequences S1 (C2-C3a-C2) and S3 (C2-C3a-C3b-C3c-C4) formed on drift D1 (Figs. 9B, 13 and 14).

Previous seismic and oceanographic studies (Ercilla et al., 2016; Juan et al., 2016, 2020) indicated that drift D1 was developed by the action of the near-bottom layers of the LMW in its route towards the Strait of Gibraltar (Fig. 14). Following the palaeo-estimation of flow regimes for the Alboran contourites by Alonso et al. (2021), we tentatively propose palaeo-flow velocities <23 cm/s for S1 and approximately 23–36 cm/s for S3. Coarse-grained sediments of both sequences (siltier to sandier deposits) are similar to other contourite drifts in shallow straits, narrow moats, and passageways (Eberli and Betzler, 2019; Rebesco et al., 2014); in contrast, drift D1 is not located in those particular settings but in an open continental slope. Oceanographic (Béranger et al., 2005), morpho-seismic and sedimentological (Ercilla et al., 2019) studies have suggested that LMW accelerates near the Strait of Gibraltar, specifically in the margin of the study area, where it is morphologically confined by the narrowing of the Alboran Sea. This acceleration would explain the overall dominance of coarser sediment in this drift and the lack of the muddy C1 division, suggesting an important winnowing of the fine particles.

The percentage of coarser grains in contourites depends on current intensity (Stow and Faugères, 2008) and sediment availability (Gonthier

et al., 1984; Rebesco et al., 2014). A relatively major presence of coarser sediment in D1 drift due to its major proximity to the coast with respect to D2 to D4 drifts (Figs. 2C and 9B) cannot be discarded, although the resulting stratigraphy of sequences seems not to reflect variations in terrigenous input by glacioeustasy but of bottom current velocity. The age model shows that its sediments are 29.5 kyr old, which means that S1 and S3 were deposited during the last lowstand (HS3 to offset of HS1), Versilian transgression and highstand (middle-late Holocene) stages (Fig. 14). Nevertheless, the stratigraphy of sequences (bigradational S1 and S3; Fig. 13) does not reflect the sediment supply variations related to the landward migration of the coastal sources (i.e., fining upwards). A great method for the bigratadional sedimentary record of contourites is to define the factor controlling the current variability because it may embrace seasonal to glacial/interglacial variations. The physical/chemical bottom current proxies (D50, sand content and UP10 and Zr/Rb ratio) and age model indicate that the bigratadional pattern of the coarse-grained drift model is related to cold periods of millennial- (HS3, HS1 and YD) and centennial-scales during the last glacial period (LGM) and Holocene, when the LMW bottom current velocity increases (Fig. 11A). It is further significant that thicker levels with coarser grains are closer to the Strait of Gibraltar (core 7), attesting to the LMW acceleration towards it (Figs. 1 and 12B).

(ii) The fine-grained drift model is defined by the vertical stacking of bigradational sequences S2 (C1-C2-C1), topcut-out S4 (C1-C2-C3a, C3b), basecut-out S6 (C3c-C4-C5) and homogenous S7 (C3b) sequences being the most common S2 formed on drifts D2, D3, and D4 for the last 25.5 kyr (Figs. 9B, 13 and 14). Previous oceanographic and morphoseismic studies point out that drifts D2 to D4 have been formed by the action of the DMW (Fig. 14; Ercilla et al., 2016; Juan et al., 2016, 2020). The predominant muddy sediments of the C1 division and the high sedimentation rates (23 to 36.9 cm/kyr) indicate that they were deposited from suspension loads under relatively weak bottom currents during the last 25.5 kyr (Fig. 9B). This weak hydrological regime could be associated with velocities, from 4 to 11 cm/s, which have been previously established for sequence S2 in the Alboran Sea (Alonso et al., 2021) and the Gulf of Cadiz (Lebreiro et al., 2018). They agree with an average value of 2–5 cm/s in the western Alboran Sea close to drift D4 and with the velocities defined by Faugères and Mulder (2011) at the fine-grained part of contourite sequences (from 5 to 10 cm/s) and Fabres et al. (2002) from modern oceanographic data (moored array measurements).

The deposition of sequences S2, S4, S6 and S7 represents millennial- and centennial-scale interruptions of silty and sandier thin beds (up to 30 silty-sandy-fast current events -FCEs-in Fig. 12C) in the muddier sedimentation during the last 25.5 kyr that are due to an abrupt increase in DMW velocity during rapid cold periods. Sequence S4 occurred during the YD; S6 and S7 during HS2; and S2 during the LGM (from the offset of HS2 to the YD and with centennial-scale fluctuations) as well as the Holocene with centennial-scale fluctuations (Figs. 9B and 12). This fact has also been observed in other areas of Alboran Sea (Alonso et al., 2021) and the western Mediterranean (Frigola et al., 2008; Le Houedec et al., 2021; Toucanne et al., 2007).

Interestingly, our observed increase in DMW velocity during the YD (Figs. 11 and 12) does not coincide with the weak circulation of this water mass suggested from its link with the last deglacial organic rich layer (ORL) formation (14 to 7 kyr) in the Alboran Sea (Pérez-Asensio et al., 2020). These authors indicate that during the late phase of the ORL (YD to early Holocene periods), there was an enhancement or deepening of the intermediate circulation and a weakening of the deep circulation. Their analysed sediment core (HER-CG-UB6 in Pérez-Asensio et al., 2020) is located at 946 m in a seafloor area dotted by seamounts and affected today by DMW, which is topographically steered by seamounts that act as obstacles to water masses (Ercilla et al., 2016; Juan et al., 2020; Palomino et al., 2011). Therefore, the record of this core could reflect the acceleration of DMW that leads to local reworking and high sedimentation rates near the eroded zones. The mapping of elongated separated drifts at the foot of seamounts and of plastered drifts (Ercilla et al., 2016) on their lee sides attest to this local acceleration. Nevertheless, we could tentatively consider the drowning of the LMW-DMW interface at least down to 946 m, which would provoke an extension of deeper areas swept by the LMW, and therefore, drifts D2, D3 and D4 would be affected by the LMW during the YD. However, our sedimentological results do not support that hypothesis. The UP10 for cores 7 and C8 indicates that both the magnitude fluctuations and trend of the shortest (centennial) and longer (millennial) events of LMW and DMW flows are unequal during the YD and ORL (Fig. 12). This fact would be contrary to what might be expected if the same water mass affected sedimentation. Furthermore, morphoseismic studies (Ercilla et al., 2016; Juan et al., 2020) do not support this hypothesis. Bearing in mind the different resolutions of seismic profiles and sediment cores, the high-resolution morphoseismic records of the drifts do not show regional stratigraphic features (e.g., relocations in the depositional architecture, erosive unconformity) that point to the occurrence of that interface shift in the past. All these mismatches indicate that a better understanding and integration of deep-water proxies as well as new and more sediment core analyses in the contourite drifts of the Alboran Sea are needed to determine the climatic impact on LMW and DMW bottom currents.

5.2. Contourite/turbidite mixed model: another archive of the bottom current and glacioeustasy interplay

This model is defined by a stratigraphy that shows a vertical trend from turbidite (S8 and S9) to contourite/turbidite mixed (S10) to contourite (S2) sequences (Figs. 9C and 13). It occurs at the overbank of the Guadiaro Fan where turbidites and contourites alternate, as revealed by its morphoseismic images that show overbank turbidites laterally coalescing with contourites of the D3 drift (Fig. 6 in Ercilla et al., 2019). Turbidite sequences S8 and S9 show similarities with those described previously in the Alboran fans (Bozzano et al., 2009; Lebreiro and Alonso, 2000; Ercilla et al., 2019). These sequences provide good validation of the standard facies for turbidites (Bouma, 1962) togheter the presence of layers rich in organic matter and of angular/subangular quartz grains and terrigenous in the sand fraction that point out to a continental source. Based on chronostratigraphy, the turbidites were deposited during the latest Pleistocene, the mixed deposits during the YD, and the contourites during the Holocene, i.e., the turbidites and mixed sequences were deposited during the early stages of the last Versilian transgression, and the contourites were mostly deposited during the last stages of transgression and sea level highstand (Fig. 9C). This temporal distribution of sequences suggests that there is an interplay between downslope and alongslope transport balanced by glacioeustasy and related sediment supply. This glacioeustasy scenario indicates that the overbank area is characterized by the predominance of turbidity overflows when the Guadiaro River was close to the Guadiaro canyon head and fed it with high-density gravity flows (Alonso and Ercilla, 2003; Ercilla et al., 2019). This would explain the high percentage of angular and subangular quartz grains in the terrigenous sand fraction in sequences S8 and S9 (Figs. 7C and 9). These flows involve sandy silt and silty flows with heights >15 m that overflow channel margins deposited on the overbank area (Ercilla et al., 2019). During the transgression, there was a decrease in the overflow processes and a noticeable effect of the steady DMW bottom layers in the sediment transport that contributed to forming the contourite/turbidite mixed sequence S10 (Fig. 9C). Their mixed sand fraction composition (Fig. 7D) suggests that during the landward transgression, the sediment making up the gravity flows also contained fragments of molluscs and subrounded quartz grains and rock fragments similar to the relict shelf sediments (Ercilla et al., 1994). Their entrainment in the sediment gravity flows would be favoured by shelf-spillover processes on the canyon head area during the last transgression. The attenuated lamination and bioturbation (Fig. 6D) displayed by the blending sequence

could indicate slow-moving turbidity flows affected by the sluggish winnowing of bottom currents. The effect of DMW dominance during the Holocene led to contourite sequence deposition (Fig. 9C). This stratigraphy of sequences refined the contourite/turbidite mixed system defined based on seismic profiles analysis (Ercilla et al., 2019) because in addition to interbedded turbidites and contourites reflecting the interaction of both processes alternatively, the mixed sequence also points to their simultaneous activity.

5.3. LMW versus DMW flow regimes during the last 29.5 kyr

The stratigraphy of sequences of the contourite drifts here characterized (Fig. 9) has palaeoceanographic implications allowing us to infer for the first time the relative variability of the LMW versus DMW flow regimes in the Alboran Sea. Their flow regime trough times reveal similarities and differences (Figs. 11 and 12). This discussion is based mainly on the UP10 and age model results from cores 7 and C8 (Fig. 12).

5.3.1. Similarities

The similarities indicate that the LMW and DMW variations occur in parallel and reflect fluctuations at three different temporal scales, 4th order (i.e., glacial/Holocene interglacial), millennial and centennial scales (Fig. 12). The 4th-order fluctuation is demonstrated by the largest scale trend of UP10. This finding indicates a stronger intensity of LMW and DMW for the glacial period characterized by higher values of UP10 (up to 76 and 97% for cores 7 and C8, respectively; Fig. 12) and weaker values for the interglacial Holocene period inferred by lower values of UP10 (up to 66 and 52% for cores 7 and C8, respectively; Fig. 12). Regarding the millennial-scale fluctuations of LMW and DMW representing FCEs, these occur in parallel, as confirmed by the overall synchronous peaks in UP10 (Fig. 12). Examples of the major FCE that represent abrupt palaeooceanographic changes include the HSs and YD associated with cold events of the last glacial and deglacial periods. The most important abrupt oceanographic change found for the YD was an abrupt return to near-glacial temperatures in the Mediterranean region (Camuera et al., 2021) and in the high-latitude North Atlantic (Clement and Peterson, 2008). This oceanographic change for LMW and DMW is shown by the drastic increase in UP10, D50, sand content, and geochemical signature (Zr/Rb ratio; Fig. 11). These synchronous palaeoceanographic fluctuations in LMW and DMW have also been observed in other sediment cores from the Alboran Sea and NW Mediterranean (Alonso et al., 2021; Frigola et al., 2007; Toucanne et al., 2012), and they are consistent with the recently estimated enhanced contribution of eastern Mediterranean source waters flowing into the western Mediterranean during the YD (Trias-Navarro et al., 2023).

Furthermore, the FCE (maximum peaks of UP10; Fig. 12) displayed overall synchronous centennial LMW and DMW variations, although they had different magnitude changes (see 5.3.2). The overall good parallelism between the planktonic $\delta^{18}O$ content and percentage of UP10 with high/low values of UP10 and heavy/light isotope values confirms the climate control at millennial and centennial time scales since the last glacial period (Fig. 12). Climate control has also been recognized in sediments from marine records of the Mediterranean Sea, such as the Ligurian Sea (Toucanne et al., 2012), Tyrrhenian Sea (Goñi et al., 2002; Sbaffi et al., 2001), and Aegean Sea (Geraga et al., 2005), and in terrestrial sedimentary records (Camuera et al., 2021). The cyclicity of these FCEs from 0.5 kyr to 1.3 kyr agrees with the short-term flow speed variability record on several drifts of the N Atlantic region (i.e., Bianchi and McCave, 1999; Hoogakker et al., 2011). This observation may indicate the influence of N Atlantic thermohaline circulation. In particular, the cycle of 1.3 kyr may be equivalent to the cycle of 1.5 kyr described by Bond et al. (2001), which has been described previously in Alboran by several authors (Moreno et al., 2005; Rodrigo-Gámiz et al., 2014), and the cycles of 0.5 and 0.8 kyr are in agreement with the cycle of approximately 0.730 years calculated by Cacho et al. (2001) and could be equivalent to the cycle of 0.550 kyr observed by Chapman and Shackleton (2000) in the N Atlantic.

5.3.2. Differences

The main difference refers to the major overall velocity of LMW versus DMW, as inferred by the high (46–76% in core 7)/low (14–68% in core C8) values of UP10, except during HS2 when DMW also shows the highest UP10 value, reaching up to 97% (Fig. 12). Another difference comes from the comparison of the magnitude changes in velocities being lower for LMW and higher for DMW, and this occurs for both the shortest and longest FCE fluctuations (Fig. 12). This would have influenced their differences in the sedimentation rates at millennial scales, which were relatively low (< 20 cm/kyr)/high (up to 80 cm/kyr) for LMW/DMW (Fig. 3C and D). This finding agrees with Moal-Darrigade et al. (2022), whose results indicate lower sedimentation rates (average 16 cm/kyr) under the LMW (Fig. 3C). Likewise, the increase in sedimentation rate during short time periods (i.e., centennial and millennial) and the values associated with DMW have also been observed in the Gardar Drift in the N Atlantic (Bianchi and McCave, 1999), where the bottom current velocity is low-moderate (11–22 cm/s; McCave et al., 2017). The magnitude differences between the LMW and DMW highlight the high sensitivity of the fine-grained sediment (core C8) to oceanographic changes and to the influence of the core water mass location (Fig. 12). The latter may exert a crucial role in sediment grain-size transport and deposition because bottom current action is commonly more notable where the core water mass is located (Ercilla et al., 2016, 2019; Hernández-Molina et al., 2014). Thus, today, the flowing LMW core along the Spanish continental slope is found at approximately 400 mwd (Dubois-Dauphin et al., 2017; Ercilla et al., 2016; Millot, 2009), close to the situation of core 7 (478 mwd); in contrast, the flowing DMW core along the Africa margin is far from sediment core C8 (914 mwd; Fig. 1A and B). Both mentioned differences, the relative velocity and magnitude changes in velocity of LMW versus DMW, would have led to minor/higher formation of contourite sequences by the action of LMW/DMW, respectively, observed on the contourite models (Fig. 13).

Another difference is that the DMW shows ventilation events (a, b, c) during HS1 and HS2 reported in the Gulf of Cadiz (Voelker et al., 2009) and NW Mediterranean (Frigola et al., 2008), which have not been identified for the LMW (Fig. 12B and C). Events a and c are characterized by a high ventilation (i.e., increase in DMW velocity) that occurs during their early and late stages, and event b is characterized by low ventilation (i.e., decrease in DMW velocity), which occurred during their middle stages. In particular, the centennial FCEs for events a, b and c for the HS1 (Fig. 12C) would be linked with the arid climate phases identified recently on a high-resolution terrestrial record in the southern Iberian Peninsula (Camuera et al., 2021), which supports climate control. Some causes for the nonrecognition of those ventilation events for the LMW could tentatively include the more active formation of DMW (i.e., WMDW) in the Gulf of Lion during the HSs (Moal-Darrigade et al., 2022 and references therein), and/or the fine sediment is more sensitive to sediment entrainment variability by bottom current fluctuations. Nevertheless, a different sampling resolution of both cores (68 years for core C8 and 156 years for core 7) cannot be discarded. More detailed sedimentological studies and integration with other biological and chemical proxies are required to understand this discoincidence.

Another difference is that the LMW and DMW have distinct responses to the way in which the onset of glacial conditions and return to interglacial conditions occurred during the HSs, YD and Holocene cold periods. This is manifested by the different stratigraphy of sequences of the drifts (Figs. 9 and 12), whose vertical trend of facies has been explained by variations in the velocity of the transporting current over time rather than inland sediment supply. The LMW formed bigradational sequences (S1 and S3) (i.e., a bottom current of steadily increasing and then decreasing velocity), and the DMW impact is represented by bigratational (S2), topcut-out (S4) (i.e., a gradual increase, a maximum and then a sharp decrease in velocity), basecut-out (S6) (i.e., a rapid and

sudden increase and then a gradual decrease in velocity) and homogeneous (S7) sequences (i.e., rapid and sudden increase and decrease in velocity) (Figs. 9 and 12). Palaeoclimate studies in the Alboran Sea (Cacho et al., 1999) indicate that the magnitude in the temperature changes in the surface water show differences between the YD and HS events; in fact, the drop in temperature was more intense during the YD than those related to HS. The distinct impact of LMW and DMW on sedimentation suggests a scenario with a complex oceanographic response to rapid climatic changes and where the causes or triggering mechanisms of those changes would impact LMW and DMW differently. Tentatively, this result would occur because as the circulation of these water masses is driven by deep-water formation in the eastern and western Mediterranean subbasins (Skliris, 2014), the propagation of the climate signatures in the thermohaline circulation would be distinct. A major research focus for sedimentologists should be the detailed analysis of the stratigraphy of sequences in other margins of the Mediterranean Sea. This will provide new insights not only into the oceanographic response to the rapid climatic oscillations by different water masses (i.e., their ocean-climate coupling) but also to decode their triggering mechanisms.

6. Conclusions

The main aim of this work is to jointly decipher for the first time the bottom current flow regime variations in LMW versus DMW and its paleoceanographic significance in response to climatic oscillations from the last glacial period to the Holocene. An integration of chronostratigraphical, sedimentological, and compositional data from contourites formed by those water masses with ad hoc support of current meter records have been carried out in fourteen sediment cores from the NW Alboran Sea. The main conclusions of this work are described as follows:

- Eight facies, F1 to F8, are characterized. Facies F1 to F4 are interpreted as contourite sediments and belong to the C1 to C5 divisions; facies F5 to F7 are interpreted as turbidites and correspond to the Tb, Tc and Td divisions of Bouma's sequence, respectively; and facies F8 is interpreted as mixed contourite/turbidite sediments. These facies are arranged into ten sequences (S1 to S10), which define two contourite stratigraphic models (terrace and drift) and a contourite/turbidite mixed model for the Alboran Sea. These models allow decoding of the sedimentary signals of palaeocurrent strength fluctuations and their palaeoclimatic significance.
- The *contourite terrace model* (i) is characterized by coarse-grained sediments rich in glaucony and involves homogeneous and fining-upwards sequences. They contain a palaeoenvironmental archive of the interplay of the AW-LMW interface with glacioeustasy from the YD to the Holocene. The contourite drift model (ii) comprises two stratigraphic sequences: one coarser for the lower slope drift (D1) and another finer for the deeper drifts D2, D3 and D4 (base of slope to basin). The *coarse-grained drift model* involves the bigradational sequences deposited by LMW with overall fast velocities accelerating towards Strait of Gibraltar during the LGM (since 29.5 kyr) and Holocene during cold periods, at millennial (HS3, HS1, and YD) and centennial scales. The *fine-grained drift model* involves the vertical stacking of bigradational, topcut-out, basecut-out and homogenous sequences. Their deposition also represents millennial (HS2, YD)- and centennial-scale interruptions of silty and sandier thin beds in the muddier sedimentation due to an abrupt reinforcement of DMW bottom current velocity during rapid cold periods since the last 25.5 kyr.
- The *contourite/turbidite mixed model* is another archive of the bottom current and glacioeustasy interplay. This model reflects the interaction of turbidity flows and DMW bottom currents both alternatively and simultaneously. Turbidites occurred during the latest Pleistocene, contourite/turbidite mixed deposits occurred in the YD, and contourites occurred in the Holocene.
- The stratigraphy of sequences of the contourite drifts allows us to infer for the first time the relative variability in the LMW versus DMW flow regimes in the Alboran Sea, indicating similarities and differences. The similarities indicate that the LMW and DMW flow regime variations occur in parallel and reflect fluctuations at three different temporal scales, 4th order (i.e., gacial/Holocene interglacial), millennial and centennial scales. The main difference refers to the major overall velocity of LMW versus DMW, except during HS2 when DMW also increased the bottom current velocity. Another difference comes from the comparison of the magnitude changes in velocities being lower for LMW and higher for DMW. Furthermore, LMW and DMW have distinct responses to the way in which the onset of glacial conditions and return to interglacial conditions took place during the HSs, YD and Holocene cold periods.
- The contourite stratigraphic models here defined could be a useful predictive tool for other areas in the Mediterranean in order to identify the major palaeoceanographic events and correlate them throughout the continental margins of this sea. Likewise, this work evidences that the joint analysis of the LMW and DMW impact on sedimentation throughout the Mediterranean may provide new insights into their different regional palaeoceanographic responses to rapid climatic oscillations (i.e., their ocean-climate coupling) and their triggering mechanisms. In addition, our results will improve regional understanding of the dynamics at the millennial level of LMW and DMW in the formation of MOW, which influences the Atlantic Meridional overturning circulation over time.

Supplementary data to this article can be found online at https://doi.org/10.1016/j.margeo.2023.107147.

Funding

This research has been funding by the Spanish projects, FAUCES (CTM2015-65461-C2-1-R) and CONTOURIBER (Ref. CTM 2008-06399-C04).

Role of the funding source

Funding source had the role in the data collection.

Declaration of generative AI and AI-assisted technologies in the writing process

AI and AI-assisted technologies have not been used in the writing processes.

Declaration of Competing Interest

The authors declare that they have no known competing financial interests or personal relationships that could have appeared to influence the work reported in this paper.

Data availability

Data supporting this study are openly available from DIGITAL.CSIC at doi: 10.20350/digitalCSIC/15507.

Acknowledgements

The authors would like to thank the captain and crew of R/V Sarmiento de Gamboa and UTM-CSIC for their assistance during the sampling cruise. The authors sincerely thank to J.M Fortuny for technical support during the SEM analysis, as well as to Juan Alberto Jiménez-Rincón (from the University of Cadiz) and to Ana Aldarias (IEO-CSIC, Cádiz) for their assistance in data processing. We are also grateful for the 'Severo Ochoa Centre of Excellence' accreditation of ICM-CSIC

(CEX2019-000928-S). Likewise, we thank to the reviewers for their suggestions that helped us to improve the paper.

References

Alonso, B., Ercilla, G., 2003. Small turbidite systems in a complex tectonic setting (SW Mediterranean Sea): morphology and growth patterns. Mar. Pet. Geol. 19, 1225–1240. https://doi.org/10.1016/S0264-8172(03)00036-9.

Alonso, B., Comas, M., Ercilla, G., Palanques, A., 1996. Textural and mineral composition of Cenozoic sedimentary facies off the western Iberian Peninsula, Sites 897, 898, 899, and 900. In: Proceedings of the Ocean Drilling Program. A&M University Ocean Drilling Program, College Station, TX, pp. 741–754.

Alonso, B., Ercilla, G., Casas, D., Stow, D., Rodríguez-Tovar, F., Dorador, J., Hernández-Molina, F., 2016. Gravity flow deposits vs contourite deposits and the sediment provenance of the Pleistocene deposits in the Faro Drift (Gulf of Cadiz): sedimentological and geochemical approaches. Mar. Geol. 377, 77–94. https://doi.org/10.1016/j.margeo.2015.12.016.

Alonso, B., Juan, C., Ercilla, G., Cacho, I., López-González, N., Rodríquez-Tovar, F.J., Dorador, J., Francés, G., Casas, D., Vandorpe, T., Vázquez, J.T., 2021. Paleoceanographic and paleoclimatic variability in the western Mediterranean during the last 25 cal. kyr BP. New insights from contourite drifts. Mar. Geol. 437 https://doi.org/10.1016/j.margeo.2021.106488, 106488.

Amorosi, A., 1996. Detecting compositional, spatial, and temporal attributes of glaucony: a tool for provenance research. Sediment. Geol. 109, 135–153. https://doi.org/10.1016/S0037-0738(96)00042-5.

Ausín, B., Flores, J.A., Sierro, F.J., Bárcena, M.A., Hernández-Almeida, I., Francés, G., Gutiérrez-Arnillas, E., Martrat, B., Grimalt, J.O., Cacho, I., 2015. Coccolithophore productivity and surface water dynamics in the Alboran Sea during the last 25kyr. Palaeogeogr. Palaeoclimatol. Palaeoecol. 418, 126–140. https://doi.org/10.1016/j.palaeo.2014.11.011.

Banerjee, S., Bansal, U., Pande, K., Meena, S.S., 2016. Compositional variability of glauconites within the Upper Cretaceous Karai Shale Formation, Cauvery Basin, India: implications for evaluation of stratigraphic condensation. Sediment. Geol. 331, 12–29. https://doi.org/10.1016/j.sedgeo.2015.10.012.

Barker, S., Diz, P., Vautravers, M.J., Pike, J., Knorr, G., Hall, I.R., Broecker, W.S., 2009. Interhemispheric Atlantic seesaw response during the last deglaciation. Nature 457, 1097–1102. https://doi.org/10.1038/nature07770.

Bazzicalupo, P., Maiorano, P., Girone, A., Marino, M., Combourieu-Nebout, N., Pelosi, N., Salgueiro, E., Incarbona, A., 2020. Holocene climate variability of the western Mediterranean: surface water dynamics inferred from calcareous plankton assemblages. Holocene 30, 691–708. https://doi.org/10.1177/0959683619895580.

Béranger, K., Mortier, L., Crépon, M., 2005. Seasonal variability of water transport through the Straits of Gibraltar, Sicily and Corsica, derived from a high-resolution model of the Mediterranean circulation. Prog. Oceanogr. 66, 341–364. https://doi.org/10.1016/j.pocean.2004.07.013.

Bianchi, G.G., McCave, I.N., 1999. Holocene periodicity in North Atlantic climate and deep-ocean flow south of Iceland. Nature 397, 515–517. https://doi.org/10.1038/17362.

Bigg, G.R., Wadley, M.R., 2001. Millennial-scale variability in the oceans: an ocean modelling view. J. Quat. Sci. 16, 309–319. https://doi.org/10.1002/jqs.599.

Blott, S.J., Pye, K., 2001. GRADISTAT: a grain size distribution and statistics package for the analysis of unconsolidated sediments. Earth Surf. Process. Landf. 26, 1237–1248. https://doi.org/10.1002/esp.261.

Bond, G., Kromer, B., Beer, J., Muscheler, R., Evans, M.N., Showers, W., Hoffmann, S., Lotti-Bond, R., Hajdas, I., Bonani, G., 2001. Persistent solar influence on North Atlantic climate during the Holocene. Science 294, 2130–2136. https://doi.org/10.1126/science.1065680.

Bouma, A.H., 1962. Sedimentology of some Flysch Deposits. Elsevier, Amsterdam, The Netherlands.

Bozzano, G., Alonso, B., Ercilla, G., Estrada, F., García, M., 2009. Late Pleistocene and Holocene depositional facies of the Almeria Channel (Alboran Sea, western Mediterranean). In: Kneller, B., Martinsen, O.J., McCaffrey, B. (Eds.), External Controls on Deep-Water Depositional Systems. SEPM Society for Sedimentary Geology, pp. 199–297. London, UK.

Cacho, I., Grimalt, J.O., Pelejero, C., Canals, M., Sierro, F.J., Flores, J.A., Shackleton, N., 1999. Dansgaard-Oeschger and Heinrich event imprints in Alboran Sea paleotemperatures. Paleoceanography 14, 698–705. https://doi.org/10.1029/1999PA900044.

Cacho, I., Grimalt, J.O., Sierro, F.J., Shackleton, N., Canals, M., 2000. Evidence for enhanced Mediterranean thermohaline circulation during rapid climatic coolings. Earth Planet. Sci. Lett. 183, 417–429. https://doi.org/10.1016/S0012-821X(00)00296-X.

Cacho, I., Grimalt, J.O., Canals, M., Sbaffi, L., Shackleton, N.J., Schönfeld, J., Zahn, R., 2001. Variability of the western Mediterranean Sea surface temperature during the last 25,000 years and its connection with the northern Hemisphere climatic changes. Paleoceanography 16, 40–52. https://doi.org/10.1029/2000PA000502.

Camuera, J., Jiménez-Moreno, G., Ramos-Román, M.J., García-Alix, A., Jiménez-Espejo, F.J., Toney, J.L., Anderson, R.S., 2021. Chronological control and centennial-scale climatic subdivisions of the last Glacial termination in the western Mediterranean region. Quat. Sci. Rev. 255, 106814. https://doi.org/10.1016/j.quascirev.2021.106814.

Carminati, E., Lustrino, M., Doglioni, C., 2012. Geodynamic evolution of the central and western Mediterranean: Tectonics vs. Igneous petrology constraints. Tectonophysics 579, 173–192. https://doi.org/10.1016/j.tecto.2012.01.026.

Català, A., Cacho, I., Frigola, J., Pena, L.D., Lirer, F., 2019. Holocene hydrography evolution in the Alboran Sea: a multi-record and multi-proxy comparison. Clim. Past 15, 927–942. https://doi.org/10.5194/cp-15-927-2019.

Chapman, M.R., Shackleton, N.J., 2000. Evidence of 550-year and 1000-year cyclicities in North Atlantic circulation patterns during the Holocene. Holocene 10, 287–291. https://doi.org/10.1191/095968300671253196.

Chiocci, F.L., Ercilla, G., Torre, J., 1997. Stratal architecture of western Mediterranean margins as the result of the stacking of Quaternary lowstand deposits below 'glacio-eustatic fluctuation base-level'. Sediment. Geol. 112, 195–217. https://doi.org/10.1016/S0037-0738(97)00035-3.

Clement, A.C., Peterson, L.C., 2008. Mechanisms of abrupt climate change of the last glacial period. Rev. Geophys. 46, RG4002 https://doi.org/10.1029/2006RG000204.

Comas, M.C., García-Dueñas, V., Jurado, M.J., 1992. Neogene tectonic evolution of the Alboran Sea from MCS data. Geo-Mar. Lett. 12, 157–164. https://doi.org/10.1007/BF02084927.

Cunningham, A.P., John, A.H., Peter, F.B., 2002. Contourite sedimentation in the Falkland Trough, western South Atlantic. In: Stow, D.A.V., Pudsey, C.J., Faugères, J. C., Viana, A.R. (Eds.), Deep-Water Contourite Systems: Modern Drifts and Ancient Series, Seismic and Sedimentary Characteristics, The Geological Society of London, pp. 337–352. London, UK.

Dansgaard, W., Johnsen, S.J., Clausen, H.B., Dahl-Jensen, D., Gundestrup, N.S., Hammer, C.U., Hvidberg, C.S., Steffensen, J.P., Sveinbjörnsdottir, A.E., Jouzel, J., Bond, G., 1993. Evidence for general instability of past climate from a 250-kyr ice-core record. Nature 364, 218–220. https://doi.org/10.1038/364218a0.

Domínguez, M., Romero, E.G., La Iglesia, A., Gascón, J., Sánchez, A., Molero, C.V., 1998. Variabilidad química y mineralogica de las facies glauconíticas del sector norte del margen continental del Mar de Alboran. Estud. Geol. 54, 17–24. https://doi.org/10.3989/egeol.98541-2202.

Dubois-Dauphin, Q., Montagna, P., Siani, G., Douville, E, Wienberg, C., Hebbeln, D., Liu, Z., Kallel, N., Dapoigny, A., Revel, M., Pons-Branchu, E., Taviani, M., Colin, Ch., 2017. Hydrological variations of the intermediate water masses of the western Mediterranean Sea during the past 20 ka inferred from neodymium isotopic composition in foraminifera and cold-water coral. Clim. Past 13, 17–37.

Eberli, G.P., Betzler, C., 2019. Characteristics of modern carbonate contourite drifts. Sedimentology 66, 1163–1191. https://doi.org/10.1111/sed.12584.

Eder, V.G., Martín-Algarra, A., Sánchez-Navas, A., Zanin, Y.N., Zamirailova, A.G., Lebedev, Y.N., 2007. Depositional controls on glaucony texture and composition, Upper Jurassic, west Siberian Basin. Sedimentology 54, 1365–1387. https://doi.org/10.1111/j.1365-3091.2007.00885.x.

Ercilla, G., 1992. Sedimentación en Márgenes Continentales y Cuencas del Mediterráneo Occidental Durante el Cuaternario (Península Ibérica). Thesis Doctoral. Universidad Politécnica de Catalunya, Barcelona, Spain.

Ercilla, G., Alonso, B., Baraza, J., 1994. Post-Calabrian sequence stratigraphy of the northwestern Alboran Sea (southwestern Mediterranean). Mar. Geol. 120, 249–265. https://doi.org/10.1016/0025-3227(94)90061-2.

Ercilla, G., Juan, C., Hernández-Molina, F.J., Bruno, M., Estrada, F., Alonso, B., Casas, D., Farran, M.L., Llave, E., García, M., Vázquez, J.T., D'Acremont, E., Gorini, C., Palomino, D., Valencia, J., El Moumni, B., Ammar, A., 2016. Significance of bottom currents in deep-sea morphodynamics: an example from the Alboran Sea. Mar. Geol. 378, 157–170. https://doi.org/10.1016/j.margeo.2015.09.007.

Ercilla, G., Juan, C., Periáñez, R., Alonso, B., Abril, J.M., Estrada, F., Casas, D., Vázquez, J.T., D'Acremont, E., Gorini, C., El Moumni, B., Do Couto, D., Valencia, J., 2019. Influence of alongslope processes on modern turbidite systems and canyons in the Alboran Sea (southwestern Mediterranean). Deep Sea Res. I Oceanogr. Res. Pap. 144, 1–16. https://doi.org/10.1016/j.dsr.2018.12.002.

Ercilla, G., Casas, D., Alonso, B., Casalbore, D., Estrada, F., Idárraga-García, J., López-González, N., Pedrosa, M., Teixeira, M., Sánchez-Guillamón, O., Azpiroz-Zabala, M., Bárcenas, P., Chiocci, F.L., García, M., Galindo-Zaldívar, J., Geyer, A., Gómez-Ballesteros, M., Juan, C., Martorelli, E., Mata, M.P., Nespereira, J., Palomino, D., Rueda, J., Vázquez, J.T., Yenes, M., 2022. Deep sea sedimentation. In: Shroder, J.F. (Ed.), Treatise on Geomorphology. Academic Press, Oxford, UK, pp. 960–988.

Fabres, J., Calafat, A., Sanchez-Vidal, A., Canals, M., Heussner, S., 2002. Composition and spatio-temporal variability of particle fluxes in the western Alboran Gyre, Mediterranean Sea. J. Mar. Syst. 33-34, 431–456. https://doi.org/10.1016/S0924-7963(02)00070-2.

Faugères, J.C., Mulder, T., 2011. Contour currents and contourite drifts. In: HüNeke, H., Mulder, T. (Eds.), Developments in Sedimentology. Elsevier, Amsterdam, Netherlands, pp. 149–214.

Faugères, J.C., Stow, D.A.V., 1993. Bottom-current-controlled sedimentation: a synthesis of the contourite problem. Sediment. Geol. 82, 287–297. https://doi.org/10.1016/0037-0738(93)90127-Q.

Faugères, J.C., Gonthier, E., Stow, D.A.V., 1984. Contourite drift molded by deep Mediterranean outflow. Geology 12, 296–300. https://doi.org/10.1130/0091-7613(1984)12<296:CDMBDM>2.0.CO;2.

Folk, R.L., Ward, W.C., 1957. Brazos River bar [Texas]; a study in the significance of grain size parameters. J. Sediment. Res. 27, 3–26. https://doi.org/10.1306/74D70646-2B21-11D7-8648000102C1865D.

Frigola, J., Moreno, A., Cacho, I., Canals, M., Sierro, F.J., Flores, J.A., Grimalt, J.O., Hodell, D.A., Curtis, J.H., 2007. Holocene climate variability in the western Mediterranean region from a deepwater sediment record. Paleoceanography 22, PA2209. https://doi.org/10.1029/2006PA001307.

Frigola, J., Moreno, A., Cacho, I., Canals, M., Sierro, F.J., Flores, J.A., Grimalt, J.O., 2008. Evidence of abrupt changes in western Mediterranean Deep Water circulation during the last 50kyr: a high-resolution marine record from the Balearic Sea. Quat. Int. 181, 88–104. https://doi.org/10.1016/j.quaint.2007.06.016.

Gascard, J.C., Richez, C., 1985. Water masses and circulation in the western Alboran Sea and in the Straits of Gibraltar. Prog. Oceanogr. 15, 157–216. https://doi.org/10.1016/0079-6611(85)90031-X.

Geraga, M., Tsaila-Monopolis, S., Ioakim, C., Papatheodorou, G., Ferentinos, G., 2005. Short-term climate changes in the southern Aegean Sea over the last 48,000 years. Palaeogeogr. Palaeoclimatol. Palaeoecol. 220, 311–332. https://doi.org/10.1016/j.palaeo.2005.01.010.

Giresse, P., 2008. Some aspects of diagenesis in contourites. In: Rebesco, M., Camerlenghi, A. (Eds.), Developments in Sedimentology. Elsevier, Amsterdam, Netherlands, pp. 203–221.

Giresse, P., Bayon, G., Tallobre, C., Loncke, L., 2021. Neodymium isotopes in glauconite for palaeoceanographic reconstructions at continental margins: a preliminary investigation from demerara rise. Front. Earth Sci. 9, 652501. https://doi.org/10.3389/feart.2021.652501.

Goñi, M.S., Cacho, I., Turon, J., Guiot, J., Sierro, F., Peypouquet, J., Grimalt, J., Shackleton, N., 2002. Synchroneity between marine and terrestrial responses to millennial scale climatic variability during the last glacial period in the Mediterranean region. Clim. Dyn. 19, 95–105. https://doi.org/10.1007/s00382-001-0212-x.

Gonthier, E.G., Faugères, J.C., Stow, D.A.V., 1984. Contourite facies of the Faro Drift, Gulf of Cadiz. In: Stow, D.A.V., Piper, D.J.W. (Eds.), Deep-Water Fine-Grained Sediments: Deep-Water Processes and Facies. Blackwell Scientific Publications, Oxford, UK, pp. 275–292.

Heaton, T.J., Köhler, P., Butzin, M., Bard, E., Reimer, R.W., Austin, W.E.N., Bronk Ramsey, C., Grootes, P.M., Hughen, K.A., Kromer, B., Reimer, P.J., Adkins, J., Burke, A., Cook, M.S., Olsen, J., Skinner, L.C., 2020. Marine20—the marine radiocarbon age calibration curve (0–55,000 cal BP). Radiocarbon 62, 779–820. https://doi.org/10.1017/RDC.2020.68.

Heinrich, H., 1988. Origin and consequences of cyclic ice rafting in the Northeast Atlantic Ocean during the past 130,000 years. Quat. Res. 29, 142–152. https://doi.org/10.1016/0033-5894(88)90057-9.

Hernández-Molina, F.J., Llave, E., Preu, B., Ercilla, G., Fontan, A., Bruno, M., Serra, N., Gomiz, J.J., Brackenridge, R.E., Sierro, F.J., Stow, D.A.W., García, M., Juan, C., Sandoval, N., Arnaiz, A., 2014. Contourite processes associated with the Mediterranean Outflow Water after its exit from the Strait of Gibraltar: Global and conceptual implications. Geology 42 (3), 227–230. https://doi.org/10.1130/G35083.1.

Hoogakker, B.A.A., Chapman, M.R., McCave, I.N., Hillaire-Marcel, C., Ellison, C.R.W., Hall, I.R., Telford, R.J., 2011. Dynamics of North Atlantic Deep Water masses during the Holocene. Paleoceanography 26, PA4214. https://doi.org/10.1029/2011PA002155.

Isola, J.I., Bravo, M.E., Bozzano, G., Palma, F.I., Ormazabal, J.P., Principi, S., Spoltore, D., Martin, R., Esteban, F.D., Tassone, A.A., 2021. The Late-Quaternary deposits of the Piedra Buena Terrace (Patagonian continental slope, SW Atlantic): an example of interaction between bottom currents and seafloor morphology. Mar. Geol. 435, 106459. https://doi.org/10.1016/j.margeo.2021.106459.

Jimenez-Espejo, F.J., Martinez-Ruiz, F., Sakamoto, T., Iijima, K., Gallego-Torres, D., Harada, N., 2007. Paleoenvironmental changes in the western Mediterranean since the last glacial maximum: high resolution multiproxy record from the Algero–Balearic basin. Palaeogeogr. Palaeoclimatol. Palaeoecol. 246, 292–306. https://doi.org/10.1016/j.palaeo.2006.10.005.

Jimenez-Espejo, F.J., Martinez-Ruiz, F., Rogerson, M., González-Donoso, J.M., Romero, O.E., Linares, D., Sakamoto, T., Gallego-Torres, D., Ruiz, J.L.R., Ortega-Huertas, M., Perez Claros, J.A., 2008. Detrital input, productivity fluctuations, and water mass circulation in the westernmost Mediterranean Sea since the Last Glacial Maximum. Geochem. Geophys. Geosyst. 9 https://doi.org/10.1029/2008GC002096. Q11U02.

Juan, C., Ercilla, G., Hernández-Molina, F.J., Estrada, F., Alonso, B., Casas, D., García, M., Farran, M.L., Llave, E., Palomino, D., Vázquez, J.T., Medialdea, T., Gorini, C., D'Acremont, E., El Moumni, B., Ammar, A., 2016. Seismic evidence of current-controlled sedimentation in the Alboran Sea during the Pliocene and Quaternary: palaeoceanographic implications. Mar. Geol. 378, 292–311. https://doi.org/10.1016/j.margeo.2016.01.006.

Juan, C., Ercilla, G., Estrada, F., Alonso, B., Casas, D., Vázquez, J.T., D'Acremont, E., Medialdea, T., Hernández-Molina, F.J., Gorini, C., El Moumni, B., Valencia, J., 2020. Multiple factors controlling the deep marine sedimentation of the Alboran Sea (SW Mediterranean) after the Zanclean Atlantic Mega-flood. Mar. Geol. 423, 106138. https://doi.org/10.1016/j.margeo.2020.106138.

Kinder, T.H., Parrilla, G., 1987. Yes, some of the Mediterranean outflow does come from great depth. J. Geophys. Res. Oceans 92, 2901–2906. https://doi.org/10.1029/JC092iC03p02901.

Le Houedec, S., Mojtahid, M., Ciobanu, M., Jorry, S.J., Bouhdayad, F.Z., Guyonneau, E., Sourice, S., Toucanne, S., 2021. Deglacial to Holocene environmental changes in the northern Ligurian Sea: the dual influence of regional climate variability and large-scale intermediate Mediterranean circulation. Palaeogeogr. Palaeoclimatol. Palaeoecol. 576, 110500. https://doi.org/10.1016/j.palaeo.2021.110500.

Lebreiro, S., Alonso, B., 2000. Sedimentary activity of the Guadiaro turbidite system during the last deglaciation to Holocen, SW Alboran Sea. In: EAGE Conference on Geology and Petroleum Geology of the Mediterranean and Circum-Mediterranean Basins. European Association of Geoscientists & Engineers, Malta, UK pp. P-35, 34.

Lebreiro, S.M., Antón, L., Reguera, M.I., Marzocchi, A., 2018. Paleoceanographic and climatic implications of a new Mediterranean Outflow branch in the southern Gulf of Cadiz. Quat. Sci. Rev. 197, 92–111. https://doi.org/10.1016/j.quascirev.2018.07.036.

Lobo, F.J., Ercilla, G., Fernández-Salas, L.M., Gámez, D., 2014. The Iberian Mediterranean shelves. Geol. Soc. Lond. Mem. 41, 147–170. https://doi.org/10.1144/M41.11.

López-González, N., Alonso, B., Juan, C., Ercilla, G., Bozzano, G., Cacho, I., Casas, D., Palomino, D., Vázquez, J.T., Estrada, F., Bárcenas, P., D'Acremont, E., Gorini, C., Moumni, B.E., 2019. 133,000 years of sedimentary record in a contourite drift in the western Alboran Sea: sediment sources and paleocurrent reconstruction. Geosciences 9, 345. https://doi.org/10.3390/geosciences9080345.

Macias, D., Garcia-Gorriz, E., Stips, A., 2016. The seasonal cycle of the Atlantic Jet dynamics in the Alboran Sea: direct atmospheric forcing versus Mediterranean thermohaline circulation. Ocean Dyn. 66, 137–151. https://doi.org/10.1007/s10236-015-0914-y.

Martorelli, E., Bosman, A., Casalbore, D., Chiocci, F., Conte, A.M., Di Bella, L., Ercilla, G., Falcini, F., Falco, P., Frezza, V., Gaglianone, G., Giaccio, B., Mancini, M., 2021. Mid-to-late Holocene upper slope contourite deposits off Capo Vaticano (Mediterranean Sea): high-resolution record of contourite cyclicity, bottom current variability and sandy facies. Mar. Geol. 431, 106372. https://doi.org/10.1016/j.margeo.2020.106372.

Martrat, B., Grimalt, J.O., Lopez-Martinez, C., Cacho, I., Sierro, F.J., Flores, J.A., Zahn, R., Canals, M., Curtis, J.H., Hodell, D.A., 2004. Abrupt temperature changes in the western Mediterranean over the past 250,000 years. Science 306, 1762–1765. https://doi.org/10.1126/science.1101706.

McCave, I.N., 2008. Size sorting during transport and deposition of fine sediments: Sortable silt and flow speed. In: Rebesco, M., Camerlenghi, A. (Eds.), Developments in Sedimentology. Elsevier, Amsterdam, The Netherlands, pp. 121–142.

McCave, I.N., Hall, I.R., 2006. Size sorting in marine muds: processes, pitfalls, and prospects for paleoflow-speed proxies. Geochem. Geophys. Geosyst. 7 https://doi.org/10.1029/2006GC001284. Q10N05.

McCave, I.N., Thornalley, D.J.R., Hall, I.R., 2017. Relation of sortable silt grain-size to deep-sea current speeds: calibration of the 'Mud Current Meter'. Deep Sea Res. I Oceanogr. Res. Pap. 127, 1–12. https://doi.org/10.1016/j.dsr.2017.07.003.

Millot, C., 1999. Circulation in the western Mediterranean Sea. J. Mar. Syst. 20, 423–442. https://doi.org/10.1016/S0924-7963(98)00078-5.

Millot, C., 2009. Another description of the Mediterranean Sea outflow. Prog. Oceanogr. 82, 101–124. https://doi.org/10.1016/j.pocean.2009.04.016.

Millot, C., 2013. Levantine Intermediate Water characteristics: an astounding general misunderstanding! Sci. Mar. 77, 217–232. https://doi.org/10.3989/scimar.03518.13A.

Millot, C., 2014. Heterogeneities of in- and out-flows in the Mediterranean Sea. Prog. Oceanogr. 120, 254–278. https://doi.org/10.1016/j.pocean.2013.09.007.

Millot, C., Monaco, A., 1984. Deep strong currents and sediment transport in the northwestern Mediterranean Sea. Geo-Mar. Lett. 4, 13–17. https://doi.org/10.1007/BF02237968.

Moal-Darrigade, P., Ducassou, E., Bout-Roumazeilles, V., Hanquiez, V., Perello, M.C., Mulder, T., Giraudeau, J., 2022. Source-to-sink pathways of clay minerals in the cadiz contourite system over the last 25 kyrs: the segregational role of mediterranean outflow water. Mar. Geol. 443, 106697. https://doi.org/10.1016/j.margeo.2021.106697.

Moreno, E., Thouveny, N., Delanghe, D., McCave, I.N., Shackleton, N.J., 2002. Climatic and oceanographic changes in the Northeast Atlantic reflected by magnetic properties of sediments deposited on the Portuguese margin during the last 340 ka. Earth Planet. Sci. Lett. 202, 465–480. https://doi.org/10.1016/S0012-821X(02)00787-2.

Moreno, A., Cacho, I., Canals, M., Grimalt, J.O., Sanchez-Vidal, A., 2004. Millennial-scale variability in the productivity signal from the Alboran Sea record, western Mediterranean Sea. Palaeogeogr. Palaeoclimatol. Palaeoecol. 211, 205–219. https://doi.org/10.1016/j.palaeo.2004.05.007.

Moreno, A., Cacho, I., Canals, M., Grimalt, J.O., Sánchez-Goñi, M.F., Shackleton, N., Sierro, F.J., 2005. Links between marine and atmospheric processes oscillating on a millennial time-scale. A multi-proxy study of the last 50,000yr from the Alboran Sea (western Mediterranean Sea). Quat. Sci. Rev. 24, 1623–1636. https://doi.org/10.1016/j.quascirev.2004.06.018.

Mulder, T., Faugères, J.C., Gonthier, E., 2008. Mixed turbidite–contourite systems. In: Rebesco, M., Camerlenghi, A. (Eds.), Developments in Sedimentology. Elsevier, Amsterdam, Netherlands, pp. 435–456.

Nebout, N., Peyron, O., Dormoy, I., Desprat, S., Beaudouin, C., Kotthoff, U., Marret, F., 2009. Rapid climatic variability in the West Mediterranean during the last 25 000 years from high resolution pollen data. Clim. Past 5, 503–521. https://doi.org/10.5194/cp-5-503-2009.

Nieto-Moreno, V., Martínez-Ruiz, F., Giralt, S., Jiménez-Espejo, F., Gallego-Torres, D., Rodrigo-Gámiz, M., García-Orellana, J., Ortega-Huertas, M., De Lange, G.J., 2011. Tracking climate variability in the western Mediterranean during the late Holocene: a multiproxy approach. Clim. Past 7, 1395–1414. https://doi.org/10.5194/cp-7-1395-2011.

Odin, G.S., Fullagar, P.D., 1988. Geological significance of the glaucony facies. In: Odln, G.S. (Ed.), Developments in Sedimentology. Elsevier, Amsterdam, Netherlands, pp. 295–332.

Odin, G.S., Letolle, R., 1980. Glauconitization and phosphatization environments: A tentative comparison. In: Bentor, Y.K. (Ed.), Marine Phosphorites—Geochemistry, Occurrence. Genesis. SEPM Society for Sedimentary Geology, Oklahoma, OK, pp. 227–237.

Odin, G.S., Matter, A., 1981. De glauconiarum origine. Sedimentology 28, 611–641. https://doi.org/10.1111/j.1365-3091.1981.tb01925.x.

Palomino, D., Vázquez, J.T., Ercilla, G., Alonso, B., López-González, N., Díaz-del-Río, V., 2011. Interaction between seabed morphology and water masses around the

seamounts on the Motril Marginal Plateau (Alboran Sea, western Mediterranean). Geo-Mar. Lett. 31, 465–479. https://doi.org/10.1007/s00367-011-0246-y.
Parrilla, G., Kinder, T.H., Preller, R.H., 1986. Deep and intermediate mediterranean water in the western Alboran Sea. Deep Sea Res. A. Oceanogr. Res. Pap. 33, 55–88. https://doi.org/10.1016/0198-0149(86)90108-1.
Pérez-Asensio, J.N., Frigola, J., Pena, L.D., Sierro, F.J., Reguera, M.I., Rodríguez-Tovar, F.J., Dorador, J., Asioli, A., Kuhlmann, J., Huhn, K., Cacho, I., 2020. Changes in western Mediterranean thermohaline circulation in association with a deglacial Organic Rich Layer formation in the Alboran Sea. Quat. Sci. Rev. 228, 106075. https://doi.org/10.1016/j.quascirev.2019.106075.
Pérez-Folgado, M., Sierro, F.J., Flores, J.A., Cacho, I., Grimalt, J.O., Zahn, R., Shackleton, N., 2003. Western Mediterranean planktonic foraminifera events and millennial climatic variability during the last 70 kyr. Mar. Micropaleontol. 48, 49–70. https://doi.org/10.1016/S0377-8398(02)00160-3.
Preu, B., Hernández-Molina, F.J., Violante, R., Piola, A.R., Paterlini, C.M., Schwenk, T., Voigt, I., Krastel, S., Spiess, V., 2013. Morphosedimentary and hydrographic features of the northern argentine margin: the interplay between erosive, depositional and gravitational processes and its conceptual implications. Deep Sea Res. I Oceanogr. Res. Pap. 75, 157–174. https://doi.org/10.1016/j.dsr.2012.12.013.
Ramsey, C.B., 2008. Deposition models for chronological records. Quat. Sci. Rev. 27, 42–60. https://doi.org/10.1016/j.quascirev.2007.01.019.
Ramsey, C.B., 2009. Bayesian analysis of radiocarbon dates. Radiocarbon 51, 337–360. https://doi.org/10.1017/S0033822200033865.
Rebesco, M., Carmelenghi, A., 2008. Contourites, Developments in Sedimentology 60. Elsevier, Amsterdam, Netherlands.
Rebesco, M., Camerlenghi, A., Van Loon, A.J., 2008. Contourite research: A field in full development. In: Rebesco, M., Camerlenghi, A. (Eds.), Developments in Sedimentology. Elsevier, Amsterdam, The Netherlands, pp. 1–10.
Rebesco, M., Hernández-Molina, F.J., Van Rooij, D., Wåhlin, A., 2014. Contourites and associated sediments controlled by deep-water circulation processes: state-of-the-art and future considerations. Mar. Geol. 352, 111–154. https://doi.org/10.1016/j.margeo.2014.03.011.
Reimer, P.J., Reimer, R.W., 2001. A marine reservoir correction database and on-line interface. Radiocarbon 43, 461–463. https://doi.org/10.1017/S0033822200038339.
Rodrigo-Gámiz, M., Martínez-Ruiz, F., Rodríguez-Tovar, F.J., Jiménez-Espejo, F.J., Pardo-Igúzquiza, E., 2014. Millennial- to centennial-scale climate periodicities and forcing mechanisms in the westernmost Mediterranean for the past 20,000 yr. Quat. Res. 81, 78–93. https://doi.org/10.1016/j.yqres.2013.10.009.
Rodrigo-Gámiz, M., Martínez-Ruiz, F., Rodríguez-Tovar, F.J., Pardo-Igúzquiza, E., Ortega-Huertas, M., 2018. Appraising timing response of paleoenvironmental proxies to the Bond cycle in the western Mediterranean over the last 20 kyr. Clim. Dyn. 50, 2925–2934. https://doi.org/10.1007/s00382-017-3782-y.
Rogerson, M., Rohling, E.J., Weaver, P.P.E., Murray, J.W., 2005. Glacial to interglacial changes in the settling depth of the Mediterranean Outflow plume. Paleoceanography 20, PA3007. https://doi.org/10.1029/2004PA001106.
Rogerson, M., Rohling, E.J., Bigg, G.R., Ramirez, J., 2012. Paleoceanography of the Atlantic-Mediterranean exchange: overview and first quantitative assessment of climatic forcing. Rev. Geophys. 50, RG2003 https://doi.org/10.1029/2011RG000376.
Rothwell, R.G., Croudace, I.W., 2015. Micro-XRF studies of sediment cores: A perspective on capability and application in the environmental sciences. In: Croudace, I.W., Rothwell, R.G. (Eds.), Micro-XRF Studies of Sediment Cores: Applications of a Non-Destructive Tool for the Environmental Sciences. Springer, Dordrecht, The Netherlands, pp. 1–21.
Sbaffi, L., Wezel, F.C., Kallel, N., Paterne, M., Cacho, I., Ziveri, P., Shackleton, N., 2001. Response of the pelagic environment to palaeoclimatic changes in the Central Mediterranean Sea during the late Quaternary. Mar. Geol. 178, 39–62. https://doi.org/10.1016/S0025-3227(01)00185-2.
Sierro, F.J., Hodell, D.A., Curtis, J.H., Flores, J.A., Reguera, I., Colmenero-Hidalgo, E., Bárcena, M.A., Grimalt, J.O., Cacho, I., Frigola, J., Canals, M., 2005. Impact of iceberg melting on Mediterranean thermohaline circulation during Heinrich events. Paleoceanography 20, PA2019. https://doi.org/10.1029/2004PA001051.
Skliris, N., 2014. Past, present and future patterns of the thermohaline circulation and characteristic water masses of the Mediterranean Sea. In: Goffredo, S., Dubinsky, Z. (Eds.), The Mediterranean Sea: Its History and Present Challenges. Springer, Dordrecht, Netherlands, pp. 29–48.
Stanley, D.J., Swift, D.J., Silverberg, N., James, N.P., Sutton, R.G., 1972. Late Quaternary progradation and sand spillover on the outer continental margin off Nova Scotia, Southeast Canada. Smithson. Contrib. Earth Sci. 8, 1–88. https://doi.org/10.5479/si.00810274.8.1.
Stow, D.A.V., Faugères, J.C., 2008. Contourite facies and the facies model. In: Rebesco, M., Camerlenghi, A. (Eds.), Developments in Sedimentology. Elsevier, Amsterdam, Netherlands, pp. 223–256.
Stow, D.A.V., Faugères, J.C., Gonthier, E., 1986. Facies distribution and textural variation in Faro Drift contourites: velocity fluctuation and drift growth. Mar. Geol. 72, 71–100. https://doi.org/10.1016/0025-3227(86)90100-3.
Stow, D.A.V., Hernández-Molina, F.J., Llave, E., Sayago-Gil, M., Díaz del Río, V., Branson, A., 2009. Bedform-velocity matrix: the estimation of bottom current velocity from bedform observations. Geology 37, 327–330. https://doi.org/10.1130/G25259A.1.
Stow, D., Smillie, Z., Wilkin, J., Jiawei Pan, J., Esegbue, O., Bahr, A., Ducassou, E., 2023. Anatomy of the bi-gradational contourite sequence: case study from the Gulf of Cadiz. Mar. Geol. 458 https://doi.org/10.1016/j.margeo.2023.10702.
Tallobre, C., Loncke, L., Bassetti, M.A., Giresse, P., Bayon, G., Buscail, R., De Madron, X. D., Bourrin, F., Vanhaesebroucke, M., Sotin, C., 2016. Description of a contourite depositional system on the Demerara Plateau: results from geophysical data and sediment cores. Mar. Geol. 378, 56–73. https://doi.org/10.1016/j.margeo.2016.01.003.
Tallobre, C., Giresse, P., Bassetti, M.A., Loncke, L., Bayon, G., Buscail, R., Tudryn, A., Zaragosi, S., 2019. Formation and evolution of glauconite in the Demerara Contourite depositional system related to NADW circulation changes during late Quaternary (French Guiana). J. S. Am. Earth Sci. 92, 167–183. https://doi.org/10.1016/j.jsames.2019.03.011.
Toucanne, S., Mulder, T., Schönfeld, J., Hanquiez, V., Gonthier, E., Duprat, J., Cremer, M., Zaragosi, S., 2007. Contourites of the Gulf of Cadiz: a high-resolution record of the paleocirculation of the Mediterranean outflow water during the last 50,000 years. Palaeogeogr. Palaeoclimatol. Palaeoecol. 246, 354–366. https://doi.org/10.1016/j.palaeo.2006.10.007.
Toucanne, S., Jouet, G., Ducassou, E., Bassetti, M.A., Dennielou, B., Minto'o, C.M.A., Lahmi, M., Touyet, N., Charlier, K., Lericolais, G., Mulder, T., 2012. A 130,000-year record of Levantine Intermediate Water flow variability in the Corsica Trough, western Mediterranean Sea. Quat. Sci. Rev. 33, 55–73. https://doi.org/10.1016/j.quascirev.2011.11.020.
Trias-Navarro, S., Pena, L.D., De la Fuente, M., Paredes, E., Garcia-Solsona, E., Frigola, J., Català, A., Caruso, A., Lirer, F., Haghipour, N., Pérez-Asensio, J., Cacho, I., 2023. Eastern Mediterranean water outflow during the Younger Dryas was twice that of the present day. Commun. Earth Environ. 4, 144. https://doi.org/10.1038/s43247-023-00812-71-9.
Van Rooij, D., Blamart, D., Kozachenko, M., Henriet, J.P., 2007. Small mounded contourite drifts associated with deep-water coral banks, Porcupine Seabight, NE Atlantic Ocean. In: Viana, A.R., Rebesco, M. (Eds.), Economic and Palaeoceanographic Significance of Contourite Deposits, The Geological Society of London, pp. 225–244. London, UK.
Vázquez, J.T., Ercilla, G., Catalán, M., Do Couto, D., Estrada, F., Galindo-Zaldívar, J., Juan, C., Palomino, D., Vegas, R., Alonso, B., Chalouan, A., Ammar, A., Azzouz, O., Benmakhlouf, M., D'Acremont, E., Gorini, C., Martos, Y., De Galdeano, C.S., 2021. A geological history for the Alboran Sea Region. In: Báez, J.C., Vázquez, J.T., Camiñas, J.A., Idrissi, M.M. (Eds.), Alboran Sea – Ecosystems and Marine Resources. Springer, Cham, Switzerland, pp. 111–155.
Viana, A.R., 2007. Seismic expression of shallow- to deep-water contourites along the south-eastern Brazilian margin. Mar. Geophys. Res. 22, 509–521. https://doi.org/10.1023/A:1016307918182.
Voelker, A.H.L., De Abreu, L., Schönfeld, J., Erlenkeuser, H., Abrantes, F., 2009. Hydrographic conditions along the western Iberian margin during marine isotope stage 2. Geochem. Geophys. Geosyst. 10 https://doi.org/10.1029/2009GC002605. Q12U08.
Yenes, M., Casas, D., Nespereira, J., López-González, N., Casalbore, D., Monterrubio, S., Alonso, B., Ercilla, G., Juan, C., Bárcenas, P., Palomino, D., Mata, P., Martínez-Díaz, P., Pérez, N., Vázquez, J.T., Estrada, F., Azpiroz-Zabala, M., Teixeira, M., 2021. The Guadiaro-Baños contourite drifts (SW Mediterranean). A geotechnical approach to stability analysis. Mar. Geol. 437 https://doi.org/10.1016/j.margeo.2021.106505, 106505.